---

**Article:**
Lermyte, F and Sobott, F orcid.org/0000-0001-9029-1865 (2017) A broader view on ion heating in traveling-wave devices using fragmentation of CsI clusters and extent of H˙ migration as molecular thermometers. Analyst, 142 (18). pp. 3388-3399. ISSN 0003-2654

https://doi.org/10.1039/c7an00161d

---

# A broader view on ion heating in traveling-wave devices using fragmentation of CsI clusters and extent of H• migration as molecular thermometers

Frederik Lermyte[1,2,3], Frank Sobott[1,4,5]*

[1]Biomolecular & Analytical Mass Spectrometry Group, Department of Chemistry, University of Antwerp, Antwerp, Belgium

[2]Centre for Proteomics, University of Antwerp, Antwerp, Belgium

[3]School of Engineering, University of Warwick, Coventry CV4 7AL, United Kingdom

[4]Astbury Centre for Structural Molecular Biology, University of Leeds, Leeds LS2 9JT, United Kingdom

[5]School of Molecular and Cellular Biology, University of Leeds, LS2 9JT, United Kingdom

*Corresponding author at: Groenenborgerlaan 171, 2020 Antwerpen, Belgium; e-mail: frank.sobott@uantwerpen.be

**Abstract**

Electron transfer dissociation (ETD) is becoming increasingly important in mass spectrometry-based analysis of peptides and proteins. Supplemental collisional activation of undissociated electron transfer products can significantly increase fragmentation yield and sequence coverage, but hydrogen rearrangements – specifically, transfer of a hydrogen radical from a *c* to a *z* fragment – lead to distorted isotope distributions and increased potential for signal overlap. Concomitant collisional activation during the ion/ion reaction significantly reduces these rearrangements, but, in ion traps, also leads to lower reaction rates and reduced overlap of anion and cation clouds. In traveling-wave ion mobility devices, it has been reported – although not under ETD conditions – that significant ion activation can occur depending on the T-wave height and velocity. Here, we investigate this phenomenon in more detail using a commercial instrument (Waters Synapt G2) and report that a similar effect can be induced within the traveling-wave Trap cell where the ETD reaction occurs, using fairly typical T-wave settings. This ion 'heating' is demonstrated by analyzing the observed isotope distributions (sensitive to the aforementioned hydrogen rearrangements) of ETD fragments of ubiquitin and substance P. A more detailed investigation of ion activation using cesium iodide clusters (without ETD reagent anions present) shows that the observed behavior is consistent with the known dynamics of ions within traveling-wave devices. The insights gained in this work are potentially relevant both for 'native ETD' studies (in which tuning needs to be optimized to avoid unintentional ion activation) as well as the design of future T-wave ETD devices (where this 'heating' effect might be exploited to promote fragment release).

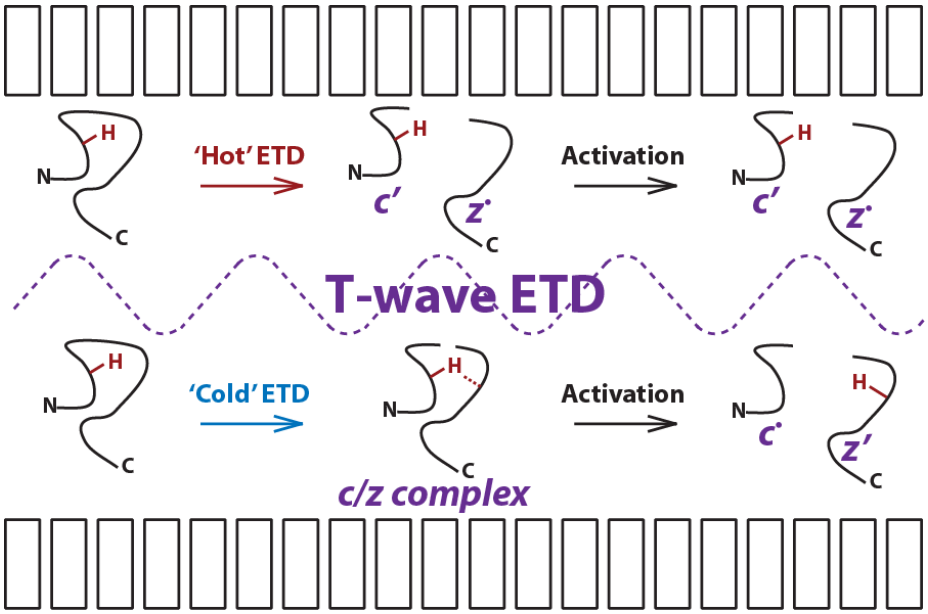
'Hot' ETD
Activation
T-wave ETD
'Cold' ETD
Activation
c/z complex

## Introduction

*Use of concomitant ion activation in ETD experiments*

Mass spectrometry, and in particular the use of electron-based fragmentation, continues to garner significant interest from the proteomics community, both for the capability to induce extensive top-down fragmentation while preserving post-translational modifications, as well as the potential to relate the observed fragmentation pattern to higher-order protein structure[1-7]. The fact that electron transfer dissociation (ETD) does not significantly disturb this higher-order structure also introduces a disadvantage, however, as noncovalent interactions can keep fragments bound in a long-lived *c*/*z* fragment complex, resulting in limited sequence coverage[8-10]. It is well-known in top-down protein analysis that such interactions can form during the electrospray process, even if proteins are denatured in solution, reducing fragmentation efficiency[11]. Most often, this is remedied by application of supplemental (collisional) activation, which destroys these noncovalent interactions, ideally without inducing further fragmentation of covalent bonds[12-14]. However, migration of a hydrogen radical from the *c'* to the $z^{\bullet}$ fragment (leading to the formation of a $c^{\bullet}$ and *z'* ion) is commonly observed within these relatively long-lived noncovalent ETD fragment complexes, and as such, supplemental activation of these complexes leads to products possessing a distorted (often both broadened and shifted) isotope distribution, complicating fragment assignment[9, 10, 15].

This problem can be alleviated by applying collisional ion activation during, rather than after the ETD process, immediately breaking up the noncovalent fragment complexes before hydrogen radical migration can occur. Within ion traps, however, this approach leads to a decrease in overlap between the cation and anion clouds, as well as an increase in relative velocity between both ion types. As both of these factors lead to a decrease in ETD reaction rate, this approach is generally of limited utility[16, 17]. Recent efforts by Coon and colleagues have demonstrated the use of ion activation by laser irradiation under ETD conditions, leading to increased sequence coverage and the observation of more 'natural' fragment isotope distributions[18-20].

While most ETD studies are still performed using ion traps, ETD is now also commercially available on quadrupole/time-of-flight (QTOF) instruments, well suited for analysis of native proteins and complexes. The most commonly used of these ETD-capable QTOFs is the Synapt (G2, G2-S, and G2-Si models), manufactured by Waters (Wilmslow, UK)[21, 22]. In these instruments, ETD is not carried out within a quadrupole ion trap, but in a traveling-wave (T-wave) ion guide (called the Trap cell), consisting of a series of ring electrodes and located between the quadrupole mass filter and the ion mobility (IM) cell. The IM cell in these instruments is also a T-wave cell, although both the background gas pressure and T-wave voltage ('wave height') are considerably higher than in the Trap cell in order to obtain good transmission and IM separation. It has long been known that field strengths in T-wave devices can become significant, potentially leading to ion activation, particularly under IM conditions. Previous theoretical and experimental research into this phenomenon will be briefly reviewed in the remainder of this introduction; however, to the best of the authors' knowledge, such a 'heating' effect within the other, lower-pressure T-wave cells in Synapt instruments has not previously been investigated. As the ETD reaction in these instruments is controlled by the T-wave height and velocity within the Trap cell, the possibility of field heating here is of particular interest. In this study, we will focus on the following questions:

1) Can we evaluate ion 'heating' effects across the full available range of parameters in the IM cell, and do they match anticipated ion behavior in a T-wave cell? Previous studies into these effects[23-25] have investigated only on a limited set of T-wave height/velocity combinations.

2) Does a similar ion 'heating' effect also occur in the Trap T-wave cell, with its different gas pressure and voltage regime, and how does it compare with the IM cell?

3) (a) Is there an observable effect of increased ion 'temperature' on ETD fragmentation behavior, and (b) how does it compare to either pre- or post-ETD ion activation? Previous work[18-20] has shown that ion activation concomitant with ETD can in principle lead to reduced $H^{\bullet}$ migration between *c* and *z*-type fragments, and may increase fragment yield and sequence coverage.

For addressing questions 1 and 2, we selected cesium iodide clusters (*i.e.* $(CsI)_nCs^+$ ions) as 'thermometer' ions which appear across a broad *m/z* range and allow to investigate to what extent ion 'heating' depends on mass. While we do not obtain quantitative 'temperature' values, CsI clusters exhibit many of the characteristics of conventional 'thermometer' ions (*cf. infra*), and trends observed in their dissociation behavior allow us to gain a qualitative understanding of the 'heating' effect and compare this to theory.

*Theoretical background of ion heating within traveling-wave devices*

In order to assess whether observations across the full parameter range are consistent with previously developed theory, we must first briefly describe the existing model for ion behavior in T-wave devices, including its assumptions and limitations. This framework has mostly been developed by Shvartsburg and Smith[26], and further refined by De Pauw and colleagues[23, 24]. In 2008, Shvartsburg and Smith investigated traveling-wave IM and provided a detailed mathematical treatment of the relation between T-wave parameters (height/velocity), pressure, and analytical characteristics, specifically macroscopic drift velocity $v_d$ and resolution[26]. In particular, they also describe the possibility of field heating within these devices, by a mechanism which is akin to molecular friction, and conclude that the maximum effective temperature reached due to field heating can theoretically be up to 7000 K, although they acknowledge that a few hundred K is a more realistic estimate under typical T-wave conditions. Briefly, in any type of ion mobility, the ions have an 'effective' temperature given by Equation 1[23, 27]:

$$T_{eff} = T_{gas} + \frac{M}{3k} v^2 \qquad \textbf{(Equation 1)}$$

where *M* is the ion mass, *k* is the Boltzmann constant, and *v* is the ion speed due to the electric field. In drift-tube ion mobility, where a constant, uniform electric field is used, $v = v_d$. Generally, in the case that ions reach a steady state drift velocity at each time point, it is easy to see that (Equation 2):

$$v^2 = [K_0 N_0 (E/N)]^2 \qquad \textbf{(Equation 2)}$$

where $K_0$ is the reduced mobility constant of the ion, *i.e.* measured at standard temperature and pressure, $N_0$ is the Loschmidt constant, and $(E/N)$ is the effective electric field strength (also referred to as $E_{eff}$ in the rest of this discussion) experienced by the ion, *i.e.* the ratio of the applied electric field strength and number density – proportional to pressure – of the background gas. As $K_0$ is usually

assumed to be constant for a given ion and choice of background gas, this equation predicts that $E_{eff}$ is the main tuning parameter which determines *v* and, by extension, the effective ion temperature. In the low-field limit, *v* is much smaller than the thermal motion of the ions, and, based on Equation 1, the effective ion temperature can be considered to be equal to the temperature of the gas – basically, the rate of collisional cooling is higher than that of frictional heating. However, with electric fields experienced by the ions in the IM cell of the Synapt G2 instrument up to ~100 V/cm[28] and typical pressure of 2.5 – 3.5 mbar, peak values of $E_{eff}$ close to 2e-15 V.cm² (200 Td) are expected to occur and a low-field regime does not necessarily fully explain ion behavior[24].

In practice, it has been shown that ions cannot always accommodate for the fast changes of *E* experienced in T-wave ion mobility (particularly for high wave velocities), and *v* is consequently typically somewhat lower than expected based on Equation 2[23]. In the Synapt G2 specifically[24, 28] *v*, $v_d$, and T-wave velocity *s* can be related as follows under normal operating conditions:

$$v^2 \leq v_d s \qquad \textbf{(Equation 3)}$$

However, as will be discussed in the next section, this equation does not necessarily apply under 'extreme' T-wave conditions (as some of the assumptions made in deriving Equation 3 become invalid). In particular, if very low or very high wave velocities are used, or very low wave heights, no mobility separation occurs and the above framework is not appropriate to describe the ions' behavior.

*Previous work and limitations to the model*

Previously, De Pauw and colleagues have investigated field heating within the IM cell of a Synapt G1 instrument using the survival yield of the p-methoxybenzylpyridinium ion as a 'thermometer' of sorts[23] and reported that the effective ion temperature could be varied in the range between 500 – 800 K in a T-wave dependent manner. While care must be taken when interpreting 'temperature' values measured in this way, the temperature scale obtained in this way does seem consistent with the notion of a corresponding fraction of ions having sufficient energy to fragment. Use of thermometer ions for this purpose was reviewed in some detail by Gabelica and De Pauw[29]. In the aforementioned field heating study[23], for a given background gas, De Pauw and colleagues find a good correlation between the calculated effective ion temperature and $v^2$ (calculated from the macroscopic drift velocity $v_d$ and the T-wave velocity *s*) when varying wave heights/velocities and IM gas pressures across a fairly broad (although still within or near the typical operating regime – *e.g.* maximum wave velocity of 1500 m/s) range. This is consistent with both Equation 1 and earlier results by Giles and colleagues[30], where increased declustering of $[bradykinin_n+nH]^{n+}$ ions (1061 *m/z*) was observed by varying the T-wave amplitude between 5.5 and 11.5 V in a prototype T-wave ion mobility device. However, choice of a different background gas had a profound effect on survival yield, with He leading to significantly less, and $CO_2$ and Ar leading to significantly more fragmentation compared to $N_2$ (the gas normally used in the IM cell). The product of $v^2$ and the reduced mass $\mu$ of the ion-neutral complex is proportional to the center-of-mass collision energy and, although the mass of the background gas only occurs indirectly in Equations 1-3 (as it affects the reduced mobility constant $K_0$), the calculated increase in effective ion temperature correlates fairly well with this energy across the different gases tested.

Interestingly, when Williams and colleagues investigated the possibility of ion heating within the IM region of a Synapt G2 instrument, they concluded that, in the typical operating regime, heating occurs predominantly during injection of the ions into the IM cell, rather than during IM separation[25]. Using a very low wave velocity (100 m/s) and fairly high wave height (30-40 V), significant additional heating did occur; however, the ions are pushed through the IM cell by a single wave in this regime and mobility constants can therefore not be measured. Follow-up experiments (again using substituted benzylpyridinium ions as 'thermometers') by De Pauw and colleagues using this second-generation instrument showed that the effective ion temperature scales with $v_d$ rather than $v^2$ in this case[24].

Comparing the IM cells of the Synapt G1 and G2 instruments, there seem to be three factors which could account for the different behavior observed in both cases. These are (1) the effective electric field strength $E_{eff}$, (2) the $N_2$ pressure, and (3) the manner in which the traveling waves are generated, *i.e.* the 'shape' of the waves. The maximum electric field that can be applied in the center of the stacked-ring ion guide in the Synapt G1 is around 60 V/cm, compared to 100 V/cm in the Synapt G2[28]. However, the $N_2$ pressure in the IM cell of the G1 instrument is normally only around 0.5 mbar, whereas pressures of 2.5 – 3.5 mbar are typically used in the G2 model. As a result, $E_{eff}$ in the IM cell of the G1 instrument can be expected to reach peak values as high as 600 Td, compared to 200 Td for the G2, possibly explaining why field heating during the IM separation seems to play a more important role within the older instrument. The difference in $N_2$ pressure itself likely also plays a role, as the frequency of collisions between ions and background gas molecules could have an effect on the interplay between collisional heating and cooling and whether the ions reach an equilibrium condition (*i.e.* a constant effective temperature). Indeed, De Pauw and colleagues have found that, if all other parameters are held constant, increasing the $N_2$ pressure leads to a reduced effective ion temperature in both the Synapt G1 and G2 (although this obviously also has an effect on $v_d$ and therefore $v^2$)[23, 24]. Finally, there are important differences in how potentials are applied to the ring electrodes in both instruments to produce the traveling waves. In the G1 instrument, a '2 up, 10 down' pattern (*i.e.* potential applied to one electrode pair, followed by five pairs without an applied potential, *etc.*) is used, with waves being separated by field-free zones as a result. In contrast, a '4 up, 4 down' pattern is used in the G2 instrument, resulting in waves that are adjacent (*i.e.* not separated by field-free regions)[28]. It was proposed by De Pauw and colleagues that ions experience a brief 'cool-down' during the time they spend in the field-free regions in the first-generation instrument, which do not occur in the IM cell of the G2[24]. As a result, they argue that the effective ion temperature can be expected to correlate with the frequency of collisions (proportional to $v_d$) in the second-generation Synapt, and with the center-of-mass collision energy of individual collisions (proportional to $\mu v^2$) in the first-generation instrument, matching the observed behavior.

Two additional, potentially important factors exist which are not accounted for in the framework outlined above. First of all, in addition to the potentials applied sequentially to the ring electrodes in a T-wave cell in order to generate the traveling waves, an RF voltage is superposed in order to axially focus the ions. As a result, it is at least theoretically possible that some RF heating also occurs, in particular for off-axis ions, in addition to T-wave induced heating and activation during ion injection. This is especially true for high ion currents, as space charge effects might cause the ion beam to become more diffuse, pushing ions closer to the ring electrodes (where such an effect would be expected to be more pronounced)[28, 30]. This phenomenon was recently investigated by Allen and Bush, using a modified Synapt G2 instrument in which the IM cell was filled with He instead of $N_2$,

and the separation was effected using a constant electric field rather than a traveling wave (but with the ions still being focused in the center of the ion guide using an RF voltage)[31]. They conclude that RF heating only results in a temperature increase of less than 2 K, and this effect can therefore be expected to also be quite limited on an unmodified Synapt G2 (note, though, that any such effect could be expected to increase with the mass of the background gas, and may therefore be up to seven times greater in $N_2$ than in He).

Finally, it is worth emphasizing that the traveling waves are generated by applying voltages to the ring electrodes in a discrete, binary (each electrode is either 'up' or 'down') manner. In the operating regime typically used, and investigated in previous studies, these can be adequately represented as smooth analog waves traveling at a constant velocity, *i.e.* the framework provided by Shvartsburg and Smith[26]. However, at extremely high wave velocities, it is likely that this approximation breaks down. Under these extreme conditions, it is therefore expected that the observed behavior would deviate from the theoretical background described above.

Given the limitations of the currently available theoretical framework for T-wave dependent ion heating, one of the main priorities of this work was to expand experiments described in previous studies across the full range of available T-wave parameters, in order to improve our understanding of this phenomenon. The overlap with previous reports has the additional benefit of allowing us to assess the use of fragmentation of CsI clusters as a probe for ion activation.

*Can ion heating also occur within a (low-pressure/low-wave height) T-wave ETD cell?*

With a different pressure and voltage regime (*e.g.* T-wave height), the question arises if ion 'heating' as described in the IM cell also occurs in the Trap. Based purely on theoretical considerations, we can argue that this is plausible, as well as evaluate how significant it is in comparison to the previously demonstrated effect in the IM cell (Question 2, see above). The occurrence of heating effects in the Trap T-wave cell is perhaps counterintuitive, given that the traveling waves during ETD operation are typically 100 times lower than in the ion mobility cell. However, the pressure in this cell is also about 50 times lower than in the ion mobility cell (5e-2 versus 2.5-3.5 mbar), and as such, the effective field strength in the Trap cell is expected to be around half of that in the IM cell (peak values potentially close to 100 Td), so the possibility of field heating cannot be *a priori* ignored. In addition to increasing the effective electric field, the lower pressure in the Trap compared to the IM cell can also be expected to promote ion activation, by providing a 'hotter' collision regime, as mentioned before. On the other hand, this is (over)compensated by the much lower mass of He compared to $N_2$, and overall ion activation in the Trap cell is therefore expected to be less than in the IM cell. Activation during ion injection into the Trap is also expected to be rather limited compared to the IM cell due the lower injection voltage used (4 V compared to 10 V in our experiments, see Experimental section).

Transit time (in TOF mode, *i.e.* no $N_2$ flow to the IM cell and no IM separation) in the Trap should also be considered, in order to judge whether the ions have time to undergo significant heating or cooling within this cell. Unfortunately, direct measurement of the transit time in the Trap cell is not possible. However, the idea that the ions spend a similar amount of time (*i.e.* low-millisecond range) in the Trap cell (in TOF mode) and the IM cell (in Mobility mode, *i.e.* approximately 2.5 mbar of $N_2$ in the IM cell and ions separated by mobility) is plausible from a theoretical perspective – the somewhat (*ca.*

50%) lower values for $E_{eff}$ in the Trap are compensated by (i) the increase in $K_0$ (reduced mobility constant) when measured in He compared to $N_2$ (as a result of the greater mass and polarizability of $N_2$)[27], (ii) the (typically 50-75%) lower wave velocities used in the Trap (as arrival time in T-wave IM theoretically scales with $s$)[26], and (iii) the shorter length of the Trap cell (18 cm versus 25 cm). We thus assume that, as in the IM cell, the transit time of the ions in the Trap cell is sufficient for effective ion temperatures to increase significantly.

In the current work, we investigate T-wave dependent fragmentation of $(CsI)_nCs^+$ clusters (with the ETD reagent source switched off), which is particularly significant for clusters below 1500 *m/z*, the range where ETD precursors are most often selected[32]. These experiments were performed in TOF mode, since the ion trajectories would be more ambiguous in Mobility mode (as the ions are then accumulated in the Trap for several milliseconds by application of a DC voltage to the last electrode and released as a 'packet' for IM separation). In contrast, transit time through the Trap in TOF mode depends directly on Trap T-wave settings (which we have investigated previously[33]). While the ion 'heating' effect can thus be characterized by investigating it in either the Trap or IM cell, in reality both cells will potentially contribute to the effect. Although we will not discuss this further in the current work, the possibility of ETD products undergoing additional activation in the IM cell should be kept in mind when performing an 'ETD-IM' experiment to separate fragments according to their mobility (which has been shown to be able to improve peak capacity in top-down MS[34]).

We also investigated whether ion 'heating' inside the Trap cell is reflected in the ETD fragmentation behavior (particularly the $z'/z^{\bullet}$ fragment ratio) of ubiquitin and the peptide substance P, by comparing spectra acquired under 'hot' and 'cold' conditions (Question 3). In these experiments, the effect of T-wave dependent ion activation during the ETD process was clearly evidenced by both increased (but always minor) CID fragmentation as well as somewhat more 'natural' fragment isotope distributions in the 'hot' regime. The latter is due to reduced migration of hydrogen radicals from *c* to *z* fragments (as the complex within which this migration occurs has a shorter survival time), distinct from the effect of applying collisional activation either prior to or after the ETD reaction. As has been noted previously[18, 19], reducing the complexity of observed isotope distributions provides analytical benefits, specifically by reducing the potential for peak overlap due to unnaturally broad distributions as well as allowing confirmation of product identities by fitting the entire isotopic envelope, rather than merely the monoisotopic peak[35].

**Experimental**

All experiments were performed on a Synapt G2 quadrupole/T-wave ion mobility/time-of-flight mass spectrometer equipped with ETD capabilities (Waters, Wilmslow, UK). The instrument was operated in ETD/Sensitivity mode (*i.e.* source voltages continuously switched to allow the Trap cell to be alternatingly filled with analyte cations and reagent anions, so that both species can interact, and voltages in the TOF and ion optics optimized for maximum sensitivity, at the expense of somewhat reduced resolving power), although the ETD reagent (anion) source was switched off for the analysis of CsI clusters. Analyte solutions were introduced into the mass spectrometer via nano-ESI using an in-house prepared gold-coated capillary. Settings for the analysis of CsI clusters were as follows (TOF mode – study of T-wave dependent fragmentation in the Trap cell): capillary 1.30 kV, sampling cone 100 V, extraction cone 10 V, nanoflow gas pressure 0.2 bar, Trap collision energy 4 V, Transfer

collision energy 0 V, backing pressure 4 mbar, Trap pressure 6.1e-2 mbar (He flow 20 mL/min), Transfer pressure 5.7e-3 mbar (Ar flow 1 mL/min). Settings in Mobility mode (study of T-wave dependent fragmentation in the IM cell) were similar, except for pressures, which were as follows: Trap 7.4e-2 mbar (He flow 20 mL/min), He cell 1.4e-3 mbar (He flow 140 mL/min), IM 2.5 mbar ($N_2$ flow 60 mL/min), Transfer 3.8e-2 mbar (Ar flow 4 mL/min). To minimize collisional heating during injection into the IM cell, the Trap DC bias and He cell DC were maintained at minimal voltages for transmission during these experiments, i.e. 20 and 10 V, respectively. For analysis of substance P and ubiquitin (TOF mode), settings were similar as for the CsI clusters, but the sampling and extraction cone voltages were set to 40 V and 2 V, respectively, and the backing pressure was 2.4 mbar. Bovine ubiquitin (Sigma U6253, 8.6 kDa) and substance P (Sigma S6883, 1.4 kDa) were dissolved at a concentration of 4 µM in a denaturing solution consisting of water/methanol (v/v) 50/50 with 0.1% formic acid added. Cesium iodide (Sigma 202134, 259.81 Da) was dissolved in water at a concentration of 2 mg/mL. Spectrum acquisitions lasted between 15 seconds and 10 minutes, in order to ensure sufficient intensity of the precursor and main dissociation products in order to accurately calculate survival yields (*i.e.* intensity of precursor divided by sum of intensities of precursor and fragments) as defined by[23]. For the shorter (<30 seconds) acquisitions, the variability of calculated survival yields between the 15-30 scans (acquisition rate 1 Hz) was calculated and typically less than 2%.

**Results and discussion**

*Use of CsI clusters as qualitative 'thermometer' ions*

As a first step, we wanted to assess the use of CsI clusters as thermometer ions. A representative spectrum is shown in Supplementary Figure S1a, illustrating several important points. First of all, the spectrum is dominated by $Cs^+$ and $(CsI)Cs^+$ ions and ion pairs, with larger clusters being far less common at these concentrations. This is in contrast to literature spectra acquired at significantly higher concentration (20 mg/mL), where clusters up to $(CsI)_{350}Cs^+$ were observed[36]. The advantage of the lower concentration used here is that it is rather unlikely for the observed $(CsI)_nCs^+$ signals to actually be due to $(CsI)_{2n}Cs_2^{2+}$ clusters. Further confirmation is provided by the absence of signals apparently corresponding to $(CsI)_xCs^+$ with non-integer x (which can only be accounted for by multiply charged clusters). As both cesium and iodine possess only one naturally occurring isotope, signal overlap with these large, multiply charged clusters would otherwise be difficult to identify and quantify, possibly complicating data analysis. The fragmentation behavior of these clusters is relatively simple (a requirement for potential 'thermometer' ions), and for a precursor $(CsI)_pCs^+$, fragmentation leads to the formation of smaller clusters $(CsI)_nCs^+$, with $0 \leq n < p$ (data not shown). To further assess the usefulness of these clusters as thermometer ions, we isolated several of the $(CsI)_{2\text{-}8}Cs^+$ clusters in the quadrupole and subjected them to collisional activation in the IM cell by gradually increasing the He cell DC voltage (offset with which the ions enter the IM cell). Supplementary Figure S1b shows a plot of survival yield (calculated as described in the experimental section, *i.e.* intensity of precursor divided by sum of intensities of precursor and fragments as defined by[23]) of these clusters versus this voltage, revealing the typical sigmoidal shape expected from theoretical considerations, with larger clusters surviving to somewhat higher collision energies (note though, that no

normalization for mass of the clusters has been performed). Without knowledge of the threshold energy value above which fragmentation (*i.e.* salt cluster dissociation) occurs[37], we can however only relate the survival yield of CsI clusters to a relative – rather than absolute – ion 'temperature'. As such, we can use these as 'qualitative thermometer ions', *i.e.* they inform on a relative temperature scale.

The second important feature of Supplementary Figure S1a is that the $(CsI)_{2\text{-}8}Cs^+$ clusters we focus on in this study occur in a significant intensity range (a factor of 20 difference between the most and least intense signal). Average ion currents for these clusters in the displayed spectrum were below 2000 counts/s, typical (even somewhat low) for peptide/protein analysis on this instrument. This makes it unlikely that any observed heating effect is due to space charge effects pushing ions out radially towards the ring electrodes of the T-wave cell, where the effective electric field is higher and RF heating could occur more easily[28, 30]. This is further supported by the fact that the observed T-wave dependent heating effects are consistent across different clusters, given the aforementioned significant intensity differences (note that quadrupole selection was performed in experiments where T-wave parameters were varied, so that only one ion type – *i.e.* a specific *m/z* value – is transferred to the T-wave).

*Field heating of CsI clusters in the ion mobility region of the Synapt G2*

In order to compare our results to earlier studies (which have focused primarily on T-wave IM devices), and to paint a more complete picture of the effect of field heating in the ion mobility region than has thus far been available (*i.e.* Question 1), for our first series of experiments we varied wave heights and velocities applied in the IM cell. We calculated the survival yield of the different CsI clusters selected in the quadrupole for every combination of a set of ten wave heights (2, 6, 10, 14, 18, 22, 26, 30, 34, and 38 V) and twelve wave velocities (*s*) (10, 20, 40, 80, 150, 300, 600, 1200, 2400, 3000, 3800, 6000 m/s) applied in this region. Wave heights were selected to be equally spaced across the full range (0 – 40 V) available on this instrument, while wave velocities were chosen to be approximately equidistant on a logarithmic axis, based on previous work[33]. As the behavior observed at 2400 m/s was often significantly different from that at 6000 m/s, two intermediate wave velocities (*i.e.* 3000 and 3800 m/s) were added. We focused on four clusters of $(CsI)_nCs^+$, selected in the quadrupole, with values of n being 2, 4, 6, and 8, corresponding to a mass range of 652 – 2212 Da. As these clusters are singly charged, they represent a typical *m/z* range in which large peptides and small (native) to intermediate/large (denatured) proteins occur. The resulting survival yields for $(CsI)_2Cs^+$ (652 Da) and $(CsI)_4Cs^+$ (1172 Da) are shown in Figure 1. Results for $(CsI)_6Cs^+$ (1692 Da) and $(CsI)_8Cs^+$ (2212 Da) can be found in Supplementary Figure S2. The hatched areas in these figures indicate regions which are not useful for ion mobility, as detailed in Supplementary S3[38]. Briefly, for a given wave height, use of a wave velocity which is too low results in the ions being swept through the IM cell by a single wave, so that $v_d = s$ and no mobility constant/collision cross-section can be determined. In this regime, arrival time is inversely proportional to *s*, whereas a linear correlation exists between these two quantities under normal T-wave IM conditions. On the other hand, if the wave velocity is too high (again, relative to wave height), arrival times cannot be accurately measured due to increased diffusion (resolution in T-wave IM decreases as *s* increases) and eventually by coupling of the waves with the ions becoming highly inefficient. Extracted survival

yields and drift times for some of the wave height/velocity combinations are tabulated in Supplementary Information S4.

In accordance with literature data[23, 24] and theoretical predictions[26], we find that in the 'normal' operating range (where $s >> v_d$, *i.e.* intermediate wave velocities and intermediate/high wave heights), increased $s$ leads to an increase in survival yield, as the resulting decrease in $v_d$ leads to a reduced effective ion temperature (Equation 3) and collision frequency. At extremely high values of $s$, $v_d$ is more or less constant, as 'pushing' of the ions by the wave becomes rather inefficient and no mobility separation occurs. To explain this, one could imagine the local field changing so fast that in effect, it almost appears as a 'ripple' without large net accelerating forces (note also – as mentioned previously – that traveling waves are not necessarily an appropriate way to describe the series of applied potentials in this extreme range), and the effective temperature increases with $s$. This accounts for the fairly abrupt drop of survival yield at wave velocities greater than about 2400 m/s. Similarly, at a constant wave velocity, an increase in wave height (and therefore $E_{eff}$) leads to a decreased survival yield, which is predicted by Equation 2 and is also consistent with previous work[23, 24]. As predicted by Equation 1, lower-mass clusters survive to somewhat higher wave velocities (although differences in dissociation energies between clusters – illustrated in Figure S1b – could also contribute to observed differences in T-Wave induced heating behavior). In the high-wave height/low-wave velocity range (where $s \approx v_d$ as ions are swept through the IM cell by one or a handful of waves), increased wave height leads to a significantly decreased survival yield, although the predicted increase of effective ion temperature due to field heating ($\Delta T_{IM}$; calculated according to Equation 1) is rather low. This is easily explained by significantly increased efficiency of energy transfer by the wave to the ion compared to a normal ion mobility regime. This is further supported by the observation that with increasing $s$, survival yield increases as the difference between $s$ and $v_d$ increases and we enter a true T-wave IM regime (Supplementary S4).

In Supplementary S4, the arrival times for $(CsI)_2Cs^+$, $(CsI)_4Cs^+$, and $(CsI)_6Cs^+$ have also been extracted in spectra where they result from dissociation of heavier clusters. Mostly, these drift times match those (assuming the same T-wave parameters, obviously) as when these lighter clusters were selected in the quadrupole. This is consistent with results reported by Williams and colleagues[25] and implies that heating predominantly occurs either during or shortly after injection into the ion mobility cell. At very low wave velocities combined with relatively high wave heights, *i.e.* the range where $s \approx v_d$ and no ion mobility separation occurs, fragments – which generally possess a higher mobility than the precursor – obviously share the arrival time of the precursor. Some intermediate fragment drift times are also occasionally visible, indicating fragmentation deeper in the ion mobility cell (somewhat analogous to metastable ions in TOF post-source decay). Therefore, although there is evidence for field heating within the IM cell, we observe that heating predominantly occurs either during or shortly after injection into the ion mobility cell. This can be most easily rationalized by assuming that activation due to even the minimal injection voltages used here is sufficient to induce fragmentation in part of the ion population, unless the ions are 'cooled' in the IM cell. This cooling effect is assumed to decrease under T-wave conditions where we would expect increased heating. This explains why our results are so conveniently accounted for by the theoretical arguments outlined earlier. As an answer to Question 1 posed in the Introduction, we can thus state that (1) fragmentation of CsI clusters indicates significant ion heating, dependent on T-wave parameters, and (2) in most of the available range of operating parameters this dependence can be easily – if

qualitatively – rationalized using the framework for the dynamics of ions in this type of cell provided by Shvartsburg and Smith[26], in a manner consistent with literature results using 'thermometer' ions.

*Field heating of ions within the Trap T-wave under ETD conditions*

Having established the manner in which ion heating within the IM cell depends on T-wave parameters in the preceding section, we investigated the possibility of T-wave dependent fragmentation of CsI clusters in the He-filled (in ETD mode) Trap T-wave cell (Question 2). This was conducted in exactly the same way as before, with ten T-wave heights and twelve wave velocities. As the same range of wave velocities is available as in the IM cell (although the default value of 300 m/s is used in most studies), the same values were used for this parameter. The wave height – which can in principle also be varied between 0 – 40 V in the Trap cell – is rarely raised above 2 V in practice, as the interaction between cations and anions is nearly completely inhibited at wave heights above 1.5 V[33]. As such, the wave height was varied between 0.1 and 1.9 V in increments of 0.2 V. The resulting survival yields for $(CsI)_2Cs^+$ (652 Da) and $(CsI)_4Cs^+$ (1172 Da) are plotted as contour maps in Figure 2. Results for $(CsI)_6Cs^+$ (1692 Da) and $(CsI)_8Cs^+$ (2212 Da) are shown in Supplementary Figure S5. Survival yields for some of the wave height/velocity combinations are tabulated for all four clusters in Supplementary Information S6.

As the transit time in the Trap cell is not measured, it is virtually impossible to estimate $v^2$ and the predicted (based on Equations 1 and 3) increase of effective ion temperature $\Delta T_{IM}$ under these conditions; however, we can still qualitatively explain the observed patterns based on results obtained under IM conditions in the previous section. For reasons outlined in the Introduction, the Trap cell (under ETD conditions) may be more 'IM-like' than would be intuitively expected, and this is supported by our earlier observation that ETD products are maximized at very low and very high Trap wave velocities, indicating that transit time is maximized (i.e. $v_d$ minimized) at these extremes, as in the IM cell[33]. Unlike in the IM cell, in this case it is not possible to easily verify the range of parameters where 'normal' IM behavior is observed; however, as the pressure in the Trap cell is approximately 40 times lower than in the IM cell, effective electric fields in the Trap cell for a wave height ranging between 0 and 1 V should be roughly comparable to the 0 – 40 V range in the IM cell. Due to the lower mass and polarizability of He compared to $N_2$ (resulting in higher mobilities being measured in the lighter gas) it can be expected that for a given effective field strength, the 'window' of IM-like behavior is shifted somewhat toward higher values for *s* in the Trap cell. Note, however, that the similar values for $E_{eff}$ do not imply that we expect to see the same level of ion activation in both T-wave devices; rather, the fact that survival yield in the Trap cell rarely drops below 70%, indicates that the heating effect is less efficient than in the IM cell. As explained in the Introduction, both the lower injection voltage and the lower mass (and to a lesser extent, polarizability) of the background gas likely contribute to the 'cooler' environment in the Trap cell.

In the low wave velocity range, in which, as discussed earlier, energy transfer from the traveling wave to the ion is much more efficient than in a true ion mobility regime, we do not observe significant fragmentation in the Trap. This is likely due to the much lower wave heights used (lower in all cases, in fact, than the lowest used in the IM cell) as well as the aforementioned effect of the mass of the background gas. Indeed, the effect of wave height, while still observable in the survival yields summarized in Supplementary Information S6, is far less pronounced in the Trap cell compared to

the ion mobility cell. Moving from 150 to about 1200-2400 m/s, an increase in wave velocity leads to ion heating and fragmentation for all wave heights, similar to the low wave height/high wave velocity regime in the IM cell, indicating as expected, that $v_d$ is quasi-constant and $v^2$ approximately proportional to $s$ at high wave velocities. At wave velocities above 2400 m/s, fragmentation again decreases. While we are not able to fully explain this behavior at this point, it is possible that coupling between the T-wave and the ions becomes so inefficient at these extremes, that insufficient energy is transferred to induce much fragmentation. As transmission in this range however decreases by at least an order of magnitude, particularly at low wave heights, it is not recommended to perform ETD experiments under these conditions.

In reply to Question 2, we can therefore say that a clear T-wave dependent 'heating' effect occurs in the Trap cell. This effect, while smaller than in the IM cell (mainly due to lower voltages and a lighter background gas), is systematic across the four CsI clusters used in this study. While (due to the different operating regimes) the general appearance of the contour maps shown in Figure 2 (and S5) differs from those shown in Figure 1 (and S2), the same theoretical framework can be used to rationalize our observations in most of the available range of parameters.

*Effect of concomitant ion activation on isotope patterns of ETD fragments*

Knowing that there is a clear and systematic effect of Trap T-wave parameters on the effective ion temperature and survival of CsI clusters over a relatively broad *m/z* range (with the reagent anion source switched off), we then tested whether this heating effect can also affect the ETD fragmentation behavior (mainly the average survival time of noncovalent fragment complexes and subsequently the probability of $H^{\bullet}$ migration from *c* to *z* ions) of peptides and proteins (Question 3 in our study). This is somewhat more complex than the experiments with cesium iodide clusters, as, besides ion temperature, the ion/ion interaction time in the Trap cell is also modulated by the wave height and velocity. In order to investigate this, the 11-residue peptide substance P (1.35 kDa) and the 76-residue protein ubiquitin (8.57 kDa) were introduced into the instrument and subjected to ETD conditions under 'hot' and 'cold' wave height/velocity regimes. It is perhaps not intuitively expected that similar behavior to that of salt clusters is observed for these biomolecular ions, particularly ubiquitin, which is much larger than even $(CsI)_8Cs^+$. However, it should be noted that the reduced mobility constant $K_0$ is inversely proportional to $(\Omega/z)$, where $\Omega$ is the collision cross-section of the ion. Interestingly, this ratio (measured in He) is quite similar (105 – 185 Å²/charge) for the 1+ CsI clusters, 3+ substance P, and 9+ ubiquitin that we have used in this work[39-41]. As a side note, it can be easily verified that this ratio does not vary by more than a factor of about 2.6 across all (denatured as well as native) proteins and complexes in the databases maintained by the Clemmer and Bush groups[41-45], with the minimum and maximum being 20+ (144 Å²/charge) and 3+ cytochrome c (380 Å²/charge), respectively. Meanwhile, absolute values for $\Omega$ in this dataset range between 757 (3+ insulin) and 20700 (72+ GroEL tetradecamer) Å², and charge states between 3+ (insulin; cytochrome c) and 72+ (GroEL tetradecamer). The relative invariance of the $(\Omega/z)$ ratio, while not entirely unexpected given the well-known correlation between solvent-accessible surface area and charge state obtained in electrospray ionization[46], suggests that most proteins and peptides will behave in a broadly similar manner to what we report here.

In Figure 3a, the observed cleavage sites of ubiquitin (9+ precursor selected in the quadrupole) are displayed using a constant wave height (0.30 V) and three different wave velocities (150, 300, and 1200 m/s), without (top) and with (bottom) the application of 10 V of supplemental activation in the Transfer cell (*i.e.* injection voltage into the argon-filled Transfer cell increased by 10 V). The wave height of 0.30 V was selected as this allows efficient mixing of anions and cations at all wave velocities[33]. Although care must be taken when directly comparing ion behavior in both cells, we have already noted that $E_{eff}$ in the Trap is approximately equivalent to that in the IM cell using a 40 times greater wave height. We could therefore expect the behavior of the 9+ ubiquitin ion (using a Trap T-wave height of 0.30 V in TOF mode) to be somewhat similar to that observed using an IM T-wave height (in Mobility mode) of 14 – 18 V (also taking into account the *ca.* 25% lower mobility of this ion in $N_2$ compared to He[42]). Using IM T-wave heights of 14 and 18 V, we measured the arrival time of 9+ ubiquitin (with the ETD reagent source switched off) while varying the wave velocity between 10 and 1200 m/s (Figure 4). We find that arrival times are minimal at 100 m/s (3.2 ms; wave height 14 V) and 125 m/s (2.7 ms; wave height 18 V) and then increase linearly with *s* ($R^2$ values of 0.996 and 0.999), reaching final values of 48.5 (14 V) and 28.4 (18 V) ms, respectively. We therefore conclude that in the Trap cell during our ETD experiments (using T-Wave velocities in the 150-1200 m/s range), transit time very likely increases with *s*. Further support for the increased reaction time at high wave velocity is provided by the fragment charge states: Nearly all fragments observed at a wave velocity of 1200 m/s were observed as singly charged ions, whereas using lower velocities, virtually all fragments containing more than 15 amino acid residues occurred exclusively doubly or triply charged (Supplementary S7). This indicates that, using the high wave velocity, more reaction steps (most being non-dissociative and charge-reducing) occur, again indicating a longer reaction time. As expected, sequence coverage is somewhat improved with the application of supplemental activation, although this effect is most prominent using a wave velocity of 300 m/s, which may indicate a somewhat greater proportion of noncovalent fragment complexes being formed (and thus available for dissociation *via* supplemental activation) under these 'cool' conditions.

It is important to note that, due to the IM-like conditions within the Trap cell (as discussed above, and in agreement with our earlier work[33]), both reaction time and effective ion temperature are determined by T-wave parameters in Synapt ETD. Recently, Coon and colleagues used an LTQ-Orbitrap instrument to show, in a systematic way across a range of peptides, that use of an ETD reaction time which is either lower or higher than the optimum, results in insufficient formation of ETD products or neutralization of a significant fraction of the reaction products, respectively. Both of these factors have a significant detrimental effect on signal-to-noise ratio, sequence coverage, and number of identifications[47]. The significant effect of reaction time (greater, in fact, than that of ion temperature) explains why, somewhat counter-intuitively, sequence coverage for ubiquitin in our experiments is highest using a wave velocity of 300 m/s – corresponding to an estimated reaction time of 5-10 ms based on IM measurements described in the previous paragraph – despite this being a rather 'cool' (*i.e.* suboptimal for fragment release) regime. However, evidence of increased ion activation during the ETD process is still provided by a decrease of the ratio of the intensities of $z'/z^{\bullet}$ peaks[1, 9, 10, 12]. The reason for this, as mentioned earlier, is the reduced amount of time available for hydrogen radical migration from the *c* to the *z* fragment (leading to conversion of $z^{\bullet}$ to $z'$ fragments), which occurs within long-lived noncovalent *c*/*z* fragment complexes. Results for the $z_3^+$ fragment of ubiquitin (9+ precursor selected in the quadrupole) are shown in Figure 3b. The reason for focusing on this fragment is that it is by far the most intense *z* fragment, and isotope ratios for this ion can

therefore be measured most accurately. Furthermore, for larger *z* fragments, with more than one potential charge site, the possibility of overlap with a complex of a smaller $z^{\bullet}$ fragment and a '*zIc*' internal fragment (i.e. one which has undergone backbone fragmentation twice, and thus has both a '*c* fragment-like' and a '*z* fragment-like' end[48]), cannot be ruled out *a priori*. Such a complex would have an identical isotope pattern to the corresponding *z'* fragment, complicating data analysis. As only one potential charge site (the guanidinium side chain of the R(74) residue) is present in the $z_3^+$ fragment of ubiquitin, no such ambiguity exists. Values for the increase in hydrogen radical abstraction when moving to other wave velocities are shown in red, and are the average of at least three spectra, each acquired for 5-10 minutes depending on signal intensity. As the proportion of *z'* ions is clearly lowest in the spectrum where a T-wave velocity of 1200 m/s was used (the 'hottest' region according to experiments using CsI clusters), we can state that the increased ion 'temperature' during the ETD process in this case does lead to an observable effect in the spectrum (Question 3a).

As previously mentioned, application of even a limited amount of supplemental activation (10 V) in the Transfer cell promotes significant dissociation of noncovalent *c*/*z* complexes and associated hydrogen abstraction, as is clearly visible when comparing the left- and right-hand side of Figure 3b. Both with and without supplemental activation, the $z'/z^{\bullet}$ ratio is minimized at a wave velocity of 1200 m/s, the same range where dissociation of CsI clusters was maximized. This clearly illustrates the disparate effects of ion activation within and downstream of the instrument region where electron transfer occurs, leading to significantly fewer and significantly more fragments in which $H^{\bullet}$ migration has occurred, respectively. The very large increase in $H^{\bullet}$ transfer caused by supplemental activation at a wave velocity of 300 m/s provides support for the hypothesis that more noncovalent fragment complexes are formed (and thus available for dissociation *via* supplemental activation) under these 'cool' conditions. An obvious question at this point is whether the same increase in effective ion temperature during ETD could also be achieved by 'pre-heating' the ions prior to entry into the Trap cell, which we have previously shown to have an effect on the dissociation behavior of large protein complexes[7]. We tested this by increasing the sampling cone voltage from 40 to 100 V, using wave velocities of 150 and 1200 m/s and a wave height of 0.30 V. In the former case, this led to a decrease of 9.2% in $z'/z^{\bullet}$ ratio, while in the latter case, this ratio actually increased by 10.3%. The reason for this increase is not yet fully understood, although one possibility is that an unfolded (at the sampling cone) protein collapses to a compact but non-native state (which in turn might show faster $H^{\bullet}$ migration) on the timescale of the experiment. It is clear though, that sufficient thermalization occurs between the sampling cone and the Trap cell, particularly of relatively small protein ions, so that this method of ion activation is a far less efficient way of increasing the effective ion temperature during the ETD process, compared to careful tuning of the T-wave settings. To answer Question 3b, we can therefore state that T-wave 'heating' during ETD leads to a lower $z'/z^{\bullet}$ ratio by breaking up noncovalent *c*/*z* fragment complexes before hydrogen radical migration can occur. In contrast, supplemental (post-ETD) collisional activation only destroys the long-lived fragment complexes after sufficient time has elapsed for $H^{\bullet}$ migration and therefore has the opposite effect on the $z'/z^{\bullet}$ ratio. While supplemental activation efficiently increases total ETD fragment yield and sequence coverage, the effect of 'pre-heating' ions before entry into the Trap cell is fairly limited. The three conditions thus have clearly distinguishable effects on the resulting fragment spectra.

We also wished to investigate the effect of different Trap T-wave settings on ETD of a smaller peptide. For this, we decided to reanalyze a dataset we have previously used to estimate the effect

of instrument settings on transit time and degree of ion/ion overlap[33]. In these experiments, the $[M+3H]^{3+}$ ion of substance P was selected for ETD. We focused on the four most intense C-terminal fragments, $z_5^+$, $z_6^+$, $z_7^+$, and $z_9^+$ (Figure 5). The $z_8$ and $z_{10}$ fragments cannot be observed due to the 'immunity' of P(2) and P(4) to ETD fragmentation (as 'fragments' remain bound via the pyrrolidine side chain). Trap wave velocities of 20, 300, 1750, and 2500 m/s were used. Wave height was 1.5 V, except for the spectra at 300 m/s, as a wave height of 0.7 V or higher at this wave velocity leads to an almost complete lack of cation/anion overlap[33]. As such, wave heights of 0.3 and 0.5 V were used at this wave velocity, leading to fairly similar spectra, demonstrating, as before, that wave velocity has a greater effect on effective ion temperature than wave height under low-pressure/low-wave height (compared to the IM cell) conditions. The values for increase in $H^\bullet$ abstraction on the right of this figure are the weighted average across all four displayed *z* fragments. Hydrogen radical migration is minimized at wave velocities around 1750 m/s, indicating, as before, that maximal ion activation occurs at this 'intermediate' wave velocity and decreases if this parameter is either increased or decreased. Further evidence for T-wave dependent ion heating is provided by concomitant CID fragmentation, which, while always very limited, increases under conditions indicated as being 'hot' based on both the survival yields of CsI clusters, as well as analysis of the isotope profiles of *z* fragments. To investigate this, we focused on the $b_{10}^{2+}$ fragment, which is by far the most intense CID fragment in these spectra and therefore the most reliable to quantify. At a Trap wave height/velocity of 1.5 V/1750 m/s, this fragment makes up 0.64% of the total spectral intensity. With different T-wave settings, this decreases significantly, to 0.44, 0.18, 0.49, and 0.06% at wave height/velocity of 1.5 V/20 m/s, 0.3 V/300 m/s, 0.5 V/300 m/s, and 1.5 V/2500 m/s, respectively, again indicating greater ion heating at the intermediate wave velocity. This further supports our finding (based on ETD of ubiquitin) that increased ion 'temperature' during the ETD process has observable effects on tandem MS spectra (Question 3a), mostly a decreased ratio of $z'/z^\bullet$ ions, but also an increased amount of (minor) CID products.

**Conclusions**

Traveling-wave technology has opened up new vistas in mass spectrometry, including high-transmission ion mobility and efficient electron transfer dissociation on QTOF platforms. However, careful tuning of T-wave parameters is necessary in both high- and low-pressure regions of the instrument, not only to optimize IM separation and ETD reaction rates, but also to control the effective ion temperature. While current physical models of T-wave devices adequately describe behavior in the typical operating regime, these fail under extreme conditions, particularly at very high wave velocities. In addition to more conventional 'thermometer' ions, both fragmentation of CsI clusters and (under ETD conditions) the relative abundance of (even-electron) $z'$ and (odd-electron) $z^\bullet$ ions can be used to probe ion activation, at least in a qualitative manner. Awareness of this ion 'heating' phenomenon, along with knowledge of the effect of T-wave parameters on the ions' internal energy, will no doubt prove to be a valuable means of affecting ion/ion chemistry in both native and denaturing mass spectrometry studies. Thus, the detailed picture of field heating presented here has the potential to inform future designs of traveling-wave ETD devices. At the same time, the current work illustrates that in experiments where a 'native-like' ion, particularly a low-*m/z* peptide, is subjected to ETD in Synapt instruments, care must be taken so as not to inadvertently disrupt the higher-order structure during the ETD process.

**Acknowledgments**

We thank the Research Foundation – Flanders (FWO) for funding a PhD fellowship (F.L.). The Synapt G2 mass spectrometer is funded by a grant from the Hercules Foundation – Flanders. Financial support from the Flemish Institute for Technological Research (VITO) is gratefully acknowledged. We also thank Jeff Brown and Kevin Giles (Waters) for insightful discussions concerning the dynamics of ions in a T-wave ETD device, and the reviewers for their valuable comments.

**Figure 1.** Contour map showing survival yields of (CsI)2$Cs^+$ (652 Da) and (CsI)4$Cs^+$ (1172 Da) across a wide range of different IM T-wave conditions. Hatching indicates the range where no ion mobility separation is typically observed, *i.e.* a T-wave velocity that (relative to wave height) is either too high or too low (See also Supplementary S3).

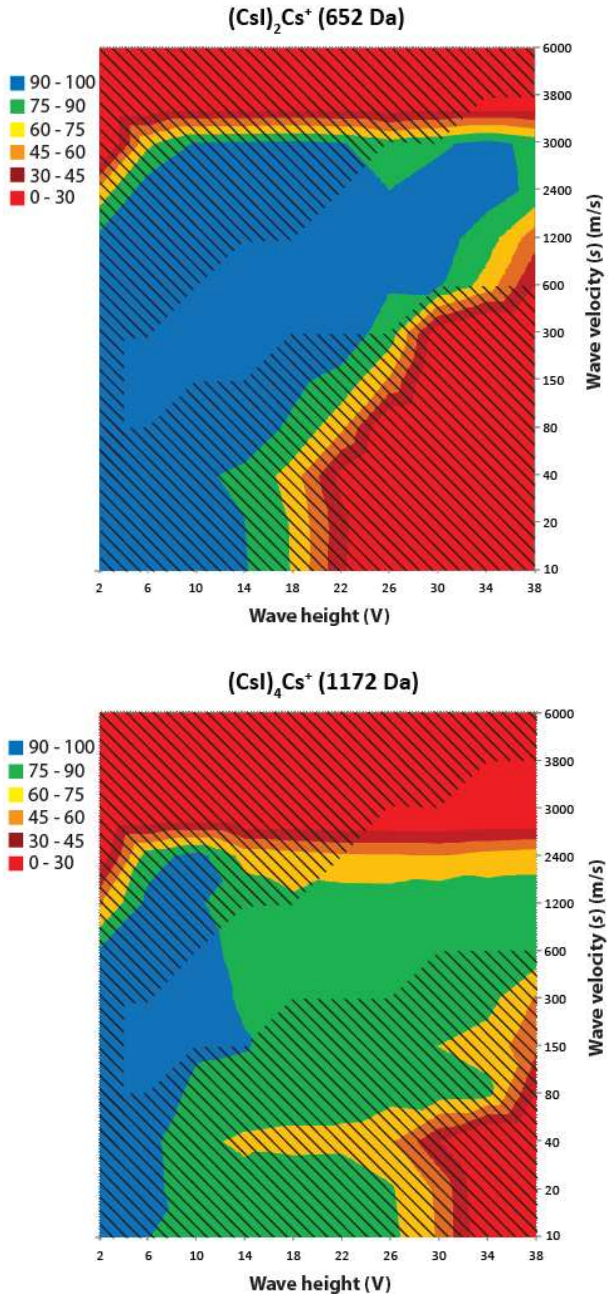

**Figure 2.** Contour map showing survival yields of $(CsI)_2Cs^+$ (652 Da) and $(CsI)_4Cs^+$ (1172 Da) across a wide range of different Trap T-wave conditions.

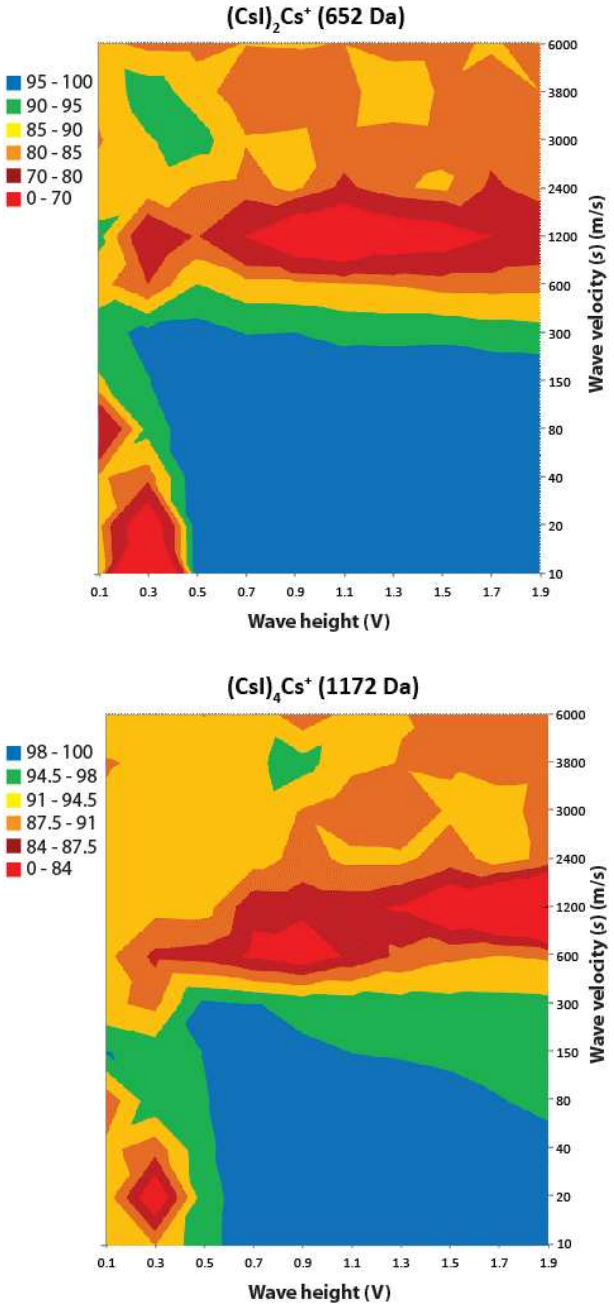

**Figure 3.** (a) Observed fragmentation sites (represented as colored sequence positions) of 9+ ubiquitin, using three different Trap T-wave velocities, with zero (top) and ten (bottom) volts of supplemental activation provided in the Transfer cell. Numbers on the left are [wave height (V)/wave velocity (m/s)]. Numbers in bold print indicate fraction of the (75) backbone N-Cα bonds cleaved. (b) Changing isotope patterns of the $z_3^+$ fragment in the spectra summarized in panel (a). Values for the increase in hydrogen radical migration shown in red are the average of at least three measurements.

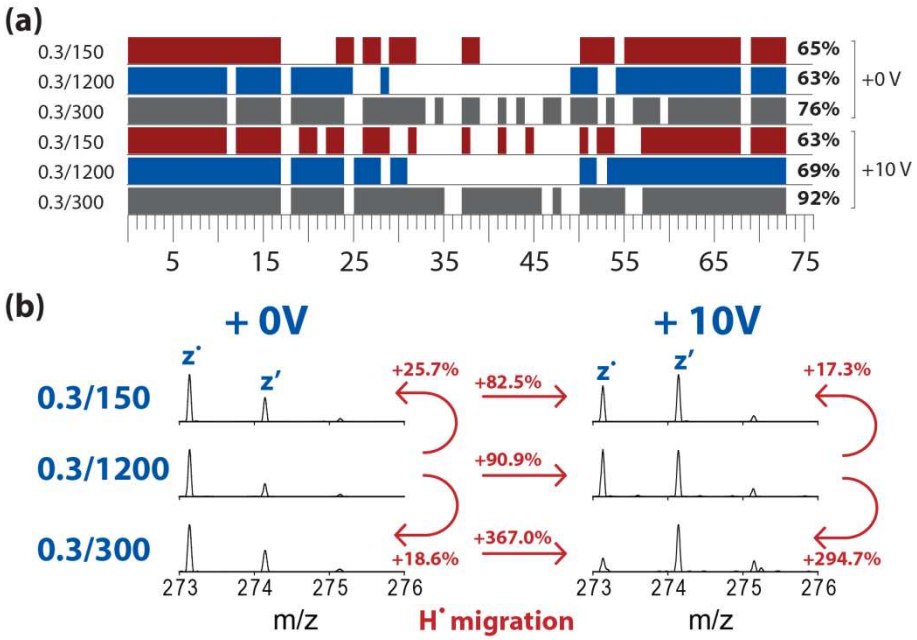

**Figure 4.** Arrival times (measured in ms) of 9+ ubiquitin across a range of T-wave velocities (m/s), with wave heights of 14 V and 18 V.

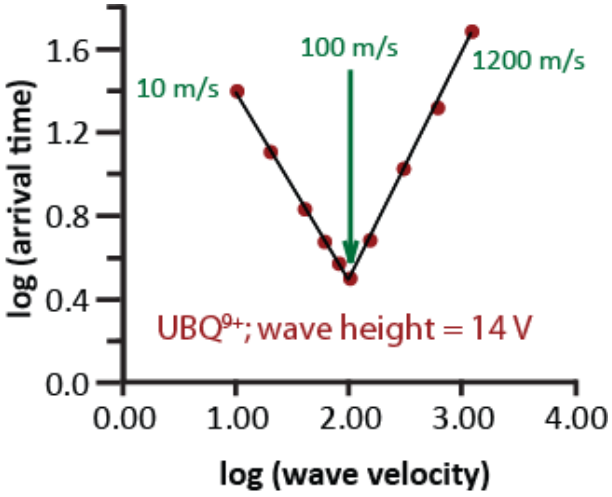


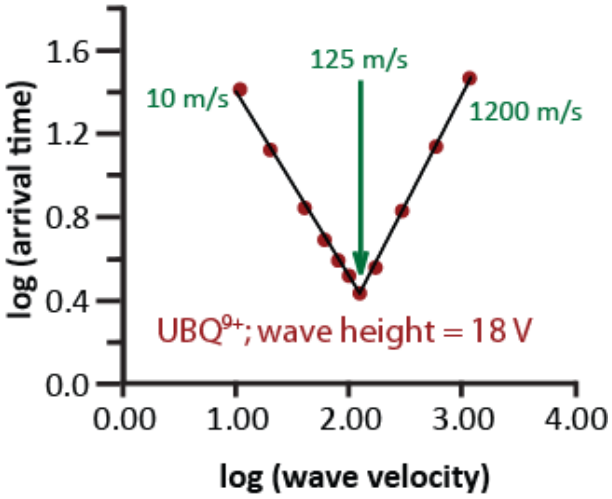

**Figure 5.** Changing isotope patterns of C-terminal fragments in ETD of substance P (3+ precursor selected) under five different sets of Trap wave height/velocity (numbers in blue in the leftmost spectra). Average increase in hydrogen radical abstraction (shown on the right) was weighted by relative intensity of the four fragments.

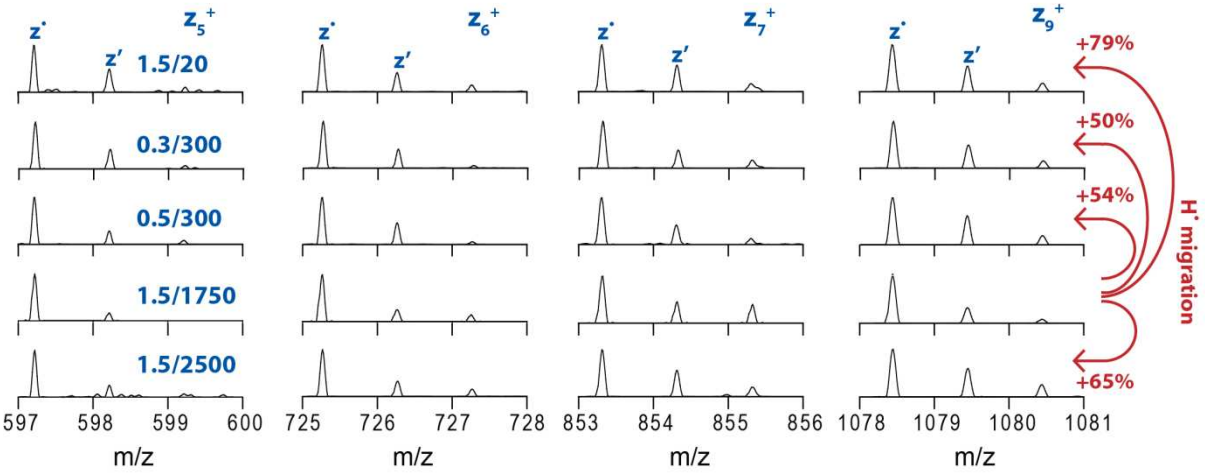

**References**


1. K. O. Zhurov, L. Fornelli, M. D. Wodrich, U. A. Laskay and Y. O. Tsybin, *Chem Soc Rev*, 2013, **42**, 5014-5030.
2. K. Breuker, H. B. Oh, D. M. Horn, B. A. Cerda and F. W. McLafferty, *J Am Chem Soc*, 2002, **124**, 6407-6420.
3. H. Oh, K. Breuker, S. K. Sze, Y. Ge, B. K. Carpenter and F. W. McLafferty, *Proc Natl Acad Sci U S A*, 2002, **99**, 15863-15868.
4. H. Zhang, W. Cui, J. Wen, R. E. Blankenship and M. L. Gross, *J Am Soc Mass Spectrom*, 2010, **21**, 1966-1968.
5. H. Zhang, W. D. Cui, J. Z. Wen, R. E. Blankenship and M. L. Gross, *Anal Chem*, 2011, **83**, 5598-5606.
6. F. Lermyte, A. Konijnenberg, J. P. Williams, J. M. Brown, D. Valkenborg and F. Sobott, *J Am Soc Mass Spectrom*, 2014, **25**, 343-350.
7. F. Lermyte and F. Sobott, *Proteomics*, 2015, **15**, 2813-2822.
8. P. B. O'Connor, C. Lin, J. J. Cournoyer, J. L. Pittman, M. Belyayev and B. A. Budnik, *J Am Soc Mass Spectrom*, 2006, **17**, 576-585.
9. Y. O. Tsybin, H. He, M. R. Emmett, C. L. Hendrickson and A. G. Marshall, *Anal Chem*, 2007, **79**, 7596-7602.
10. F. Lermyte, M. K. Łącki, D. Valkenborg, G. Baggerman, A. Gambin and F. Sobott, *Int J Mass Spectrom*, 2015, **390**, 146-154.
11. X. Han, M. Jin, K. Breuker and F. W. McLafferty, *Science*, 2006, **314**, 109-112.
12. Y. Xia, H. Han and S. A. McLuckey, *Anal Chem*, 2008, **80**, 1111-1117.
13. S. J. Pitteri, P. A. Chrisman and S. A. McLuckey, *Anal Chem*, 2005, **77**, 5662-5669.
14. D. L. Swaney, G. C. McAlister, M. Wirtala, J. C. Schwartz, J. E. Syka and J. J. Coon, *Anal Chem*, 2007, **79**, 477-485.
15. F. Lermyte, M. K. Łacki, D. Valkenborg, A. Gambin and F. Sobott, *J Am Soc Mass Spectrom*, 2017, **28**, 69-76.
16. G. E. Reid, H. Shang, J. M. Hogan, G. U. Lee and S. A. McLuckey, *J Am Chem Soc*, 2002, **124**, 7353-7362.
17. S. A. McLuckey and J. L. Stephenson, Jr., *Mass Spectrom Rev*, 1998, **17**, 369-407.
18. A. R. Ledvina, G. C. McAlister, M. W. Gardner, S. I. Smith, J. A. Madsen, J. C. Schwartz, G. C. Stafford, Jr., J. E. Syka, J. S. Brodbelt and J. J. Coon, *Angew Chem Int Ed Engl*, 2009, **48**, 8526-8528.
19. N. M. Riley, M. S. Westphall and J. J. Coon, *Anal Chem*, 2015, **87**, 7109-7116.
20. A. R. Ledvina, N. A. Beauchene, G. C. McAlister, J. E. Syka, J. C. Schwartz, J. Griep-Raming, M. S. Westphall and J. J. Coon, *Anal Chem*, 2010, **82**, 10068-10074.
21. S. D. Pringle, K. Giles, J. L. Wildgoose, J. P. Williams, S. E. Slade, K. Thalassinos, R. H. Bateman, M. T. Bowers and J. H. Scrivens, *Int J Mass Spectrom*, 2007, **261**, 1-12.
22. J. P. Williams, J. M. Brown, I. Campuzano and P. J. Sadler, *Chem Commun*, 2010, **46**, 5458-5460.
23. D. Morsa, V. Gabelica and E. De Pauw, *Anal Chem*, 2011, **83**, 5775-5782.
24. D. Morsa, V. Gabelica and E. De Pauw, *J Am Soc Mass Spectrom*, 2014, **25**, 1384-1393.
25. S. I. Merenbloom, T. G. Flick and E. R. Williams, *J Am Soc Mass Spectrom*, 2012, **23**, 553-562.
26. A. A. Shvartsburg and R. D. Smith, *Anal Chem*, 2008, **80**, 9689-9699.
27. H. E. Revercomb and E. A. Mason, *Anal Chem*, 1975, **47**, 970-983.
28. K. Giles, J. P. Williams and I. Campuzano, *Rapid Commun Mass Sp*, 2011, **25**, 1559-1566.
29. V. Gabelica and E. De Pauw, *Mass Spectrom Rev*, 2005, **24**, 566-587.
30. K. Giles, S. D. Pringle, K. R. Worthington, D. Little, J. L. Wildgoose and R. H. Bateman, *Rapid Commun Mass Sp*, 2004, **18**, 2401-2414.
31. S. J. Allen and M. F. Bush, *J. Am. Soc. Mass Spectrom.*, 2016, **27**, 2054-2063.

32. D. M. Good, M. Wirtala, G. C. McAlister and J. J. Coon, *Mol Cell Proteomics*, 2007, **6**, 1942-1951.
33. F. Lermyte, T. Verschueren, J. M. Brown, J. P. Williams, D. Valkenborg and F. Sobott, *Methods*, 2015, **89**, 22-29.
34. N. F. Zinnel, P. J. Pai and D. H. Russell, *Anal Chem*, 2012, **84**, 3390-3397.
35. L. Li and Z. Tian, *Rapid Commun Mass Spectrom*, 2013, **27**, 1267-1277.
36. F. Sobott, H. Hernandez, M. G. McCammon, M. A. Tito and C. V. Robinson, *Anal Chem*, 2002, **74**, 1402-1407.
37. C. Collette and E. De Pauw, *Rapid Commun Mass Spectrom*, 1998, **12**, 165-170.
38. C. Atmanene, S. Petiot-Bécard, D. Zeyer, A. Van Dorsselaer, V. Vivat-Hannah and S. Sanglier-Cianférani, *Anal. Chem.*, 2012, **84**, 4703-4710.
39. H. Ouyang, C. Larriba-Andaluz, D. R. Oberreit and C. J. Hogan, *J Am Soc Mass Spectr*, 2013, **24**, 1833-1847.
40. S. Lee, M. A. Ewing, F. M. Nachtigall, R. T. Kurulugama, S. J. Valentine and D. E. Clemmer, *J Phys Chem B*, 2010, **114**, 12406-12415.
41. S. J. Valentine, A. E. Counterman and D. E. Clemmer, *J Am Soc Mass Spectr*, 1997, **8**, 954-961.
42. M. F. Bush, Z. Hall, K. Giles, J. Hoyes, C. V. Robinson and B. T. Ruotolo, *Anal Chem*, 2010, **82**, 9557-9565.
43. R. Salbo, M. F. Bush, H. Naver, I. Campuzano, C. V. Robinson, I. Pettersson, T. J. Jorgensen and K. F. Haselmann, *Rapid Commun Mass Spectrom*, 2012, **26**, 1181-1193.
44. K. B. Shelimov, D. E. Clemmer, R. R. Hudgins and M. F. Jarrold, *J Am Chem Soc*, 1997, **119**, 2240-2248.
45. S. J. Valentine, J. G. Anderson, A. D. Ellington and D. E. Clemmer, *J Phys Chem B*, 1997, **101**, 3891-3900.
46. A. Konijnenberg, A. Butterer and F. Sobott, *Biochim Biophys Acta*, 2013, **1834**, 1239-1256.
47. C. M. Rose, M. J. P. Rush, N. M. Riley, A. E. Merrill, N. W. Kwiecien, D. D. Holden, C. Mullen, M. S. Westphall and J. J. Coon, *J Am Soc Mass Spectr*, 2015, **26**, 1848-1857.
48. S. R. Harvey, M. Porrini, R. C. Tyler, C. E. MacPhee, B. F. Volkman and P. E. Barran, *Phys Chem Chem Phys*, 2015, **17**, 10538-10550.

**Supplementary Information**

**Figure S1.** (a) Representative CsI spectrum, acquired using an IM wave height of 25 V and wave velocity of 500 m/s (inset shows a zoomed-in view of the 600 – 2300 *m/z* region; intensity of the $(CsI)_3Cs^+$ peak is 3.95% of that of the $Cs^+$ peak). (b) Survival yield of the four $(CsI)_nCs^+$ clusters focused on in this study as a function of He cell DC voltage (normalized to the highest value observed for each cluster across these experiments), showing a typical sigmoidal curve.

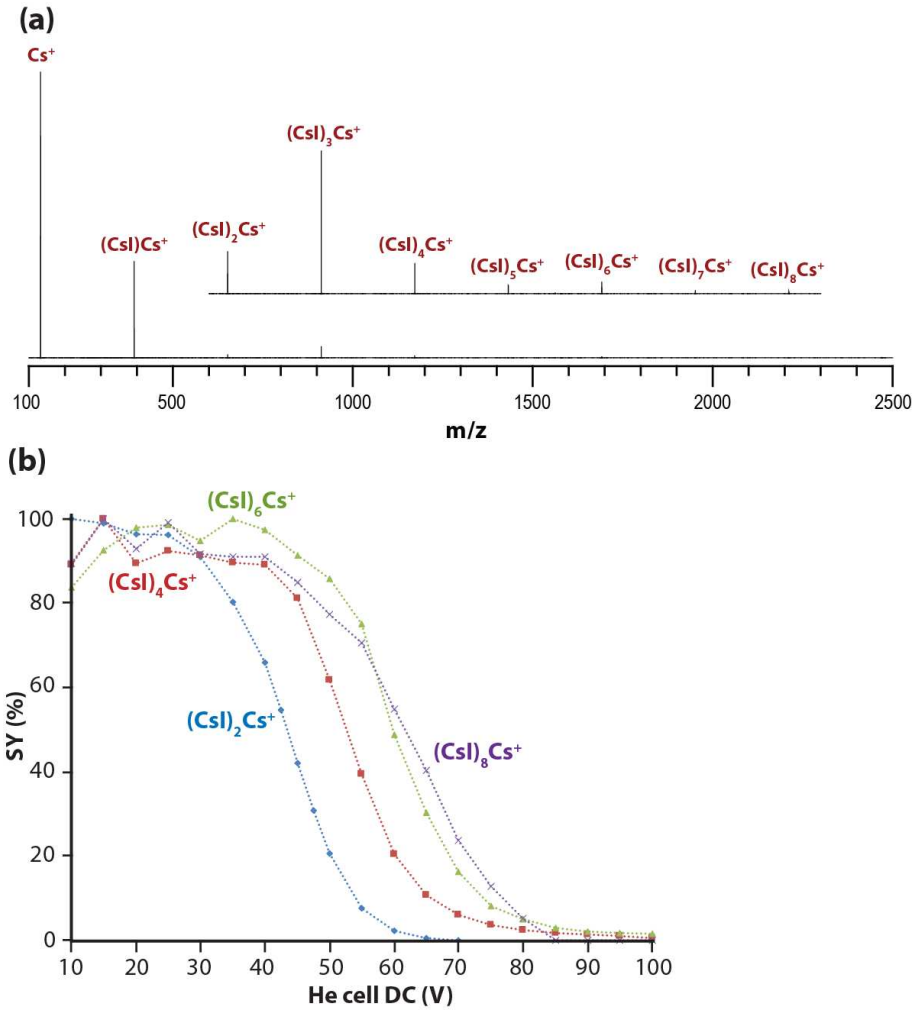

**Figure S2.** Contour map showing survival yields of $(CsI)_6Cs^+$ (1692 Da) and $(CsI)_8Cs^+$ (2212 Da) across a wide range of different IM T-wave conditions. Hatching indicates the range where no ion mobility separation is typically observed, *i.e.* T-wave wave velocity either too high or too low.

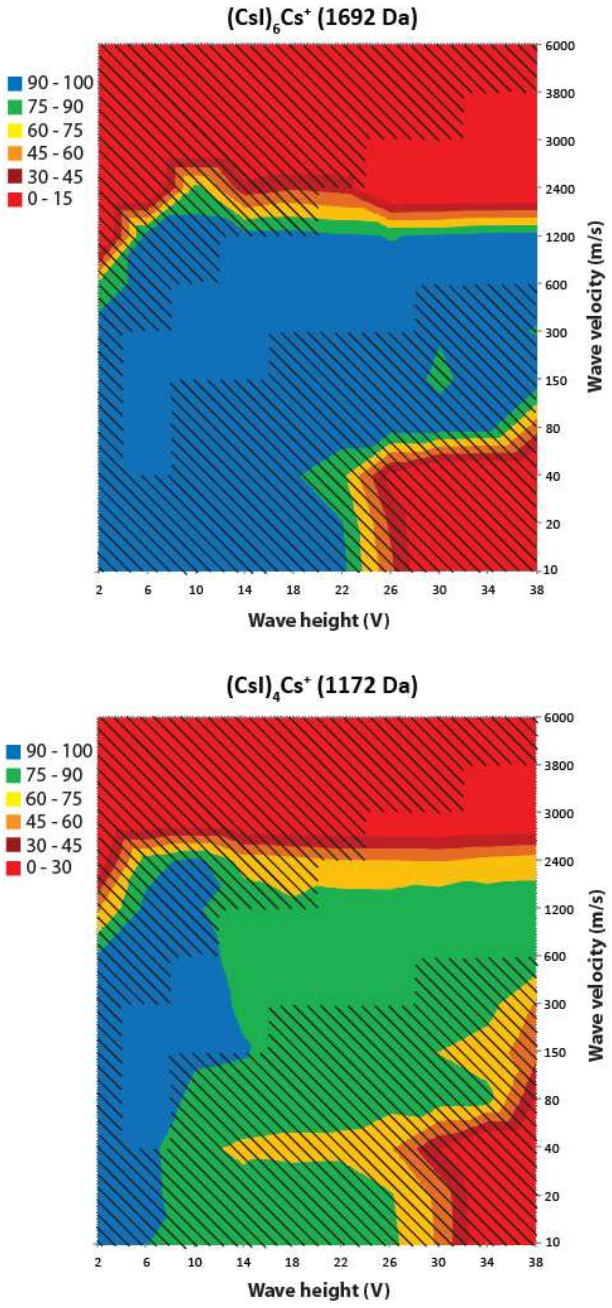

**Figure S3:** (left) arrival time distributions (Mobility mode) for $(CsI)_2Cs^+$ (652 Da) at an IM wave height of 22 V and various wave velocities; (right) plots of log (arrival time) versus log (wave velocity). The green arrow in each of these plots indicates the data point corresponding to the spectrum shown on the left. Arrival times could be reliably measured for data points shown in red (connected be a solid black line); those in blue (connected by a dashed black line) were calculated based on the observed data. Clear linear (in this log-log plot) trends (both with $R^2$ values of 0.998) in the observed data are visible in the ranges between (20 – 150 m/s) and (300 – 1200 m/s). The experiment corresponding to the data point in green (245 m/s; 1.43 ms) was not performed; rather, this is the theoretical minimum transit time calculated based on the aforementioned linear trends. As in Figures 1 and S1, hatched areas are not useful for ion mobility, either because (hatched area on the left-hand side) ions are swept through the cell by a single traveling wave (*i.e.* no mobility separation), or (hatched area on the right-hand side) arrival times could not be reliably measured (apparent 'peaks' – with very poor shape – at low arrival time for wave velocities of 2400 and 3000 m/s are due to roll-over).

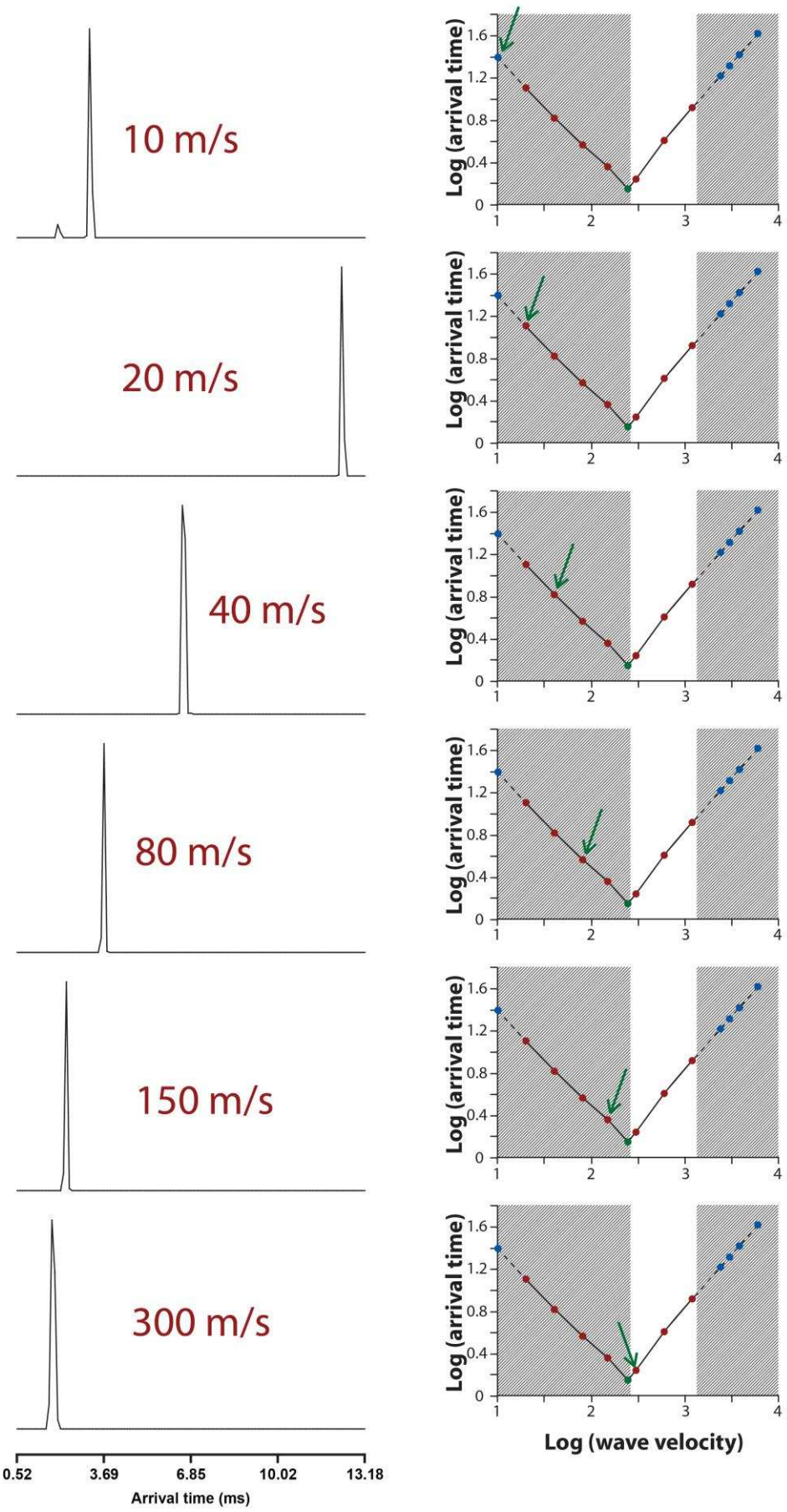
10 m/s
20 m/s
40 m/s
80 m/s
150 m/s
300 m/s
0.52
3.69
6.85
10.02
13.18
Arrival time (ms)
Log (arrival time)
Log (wave velocity)

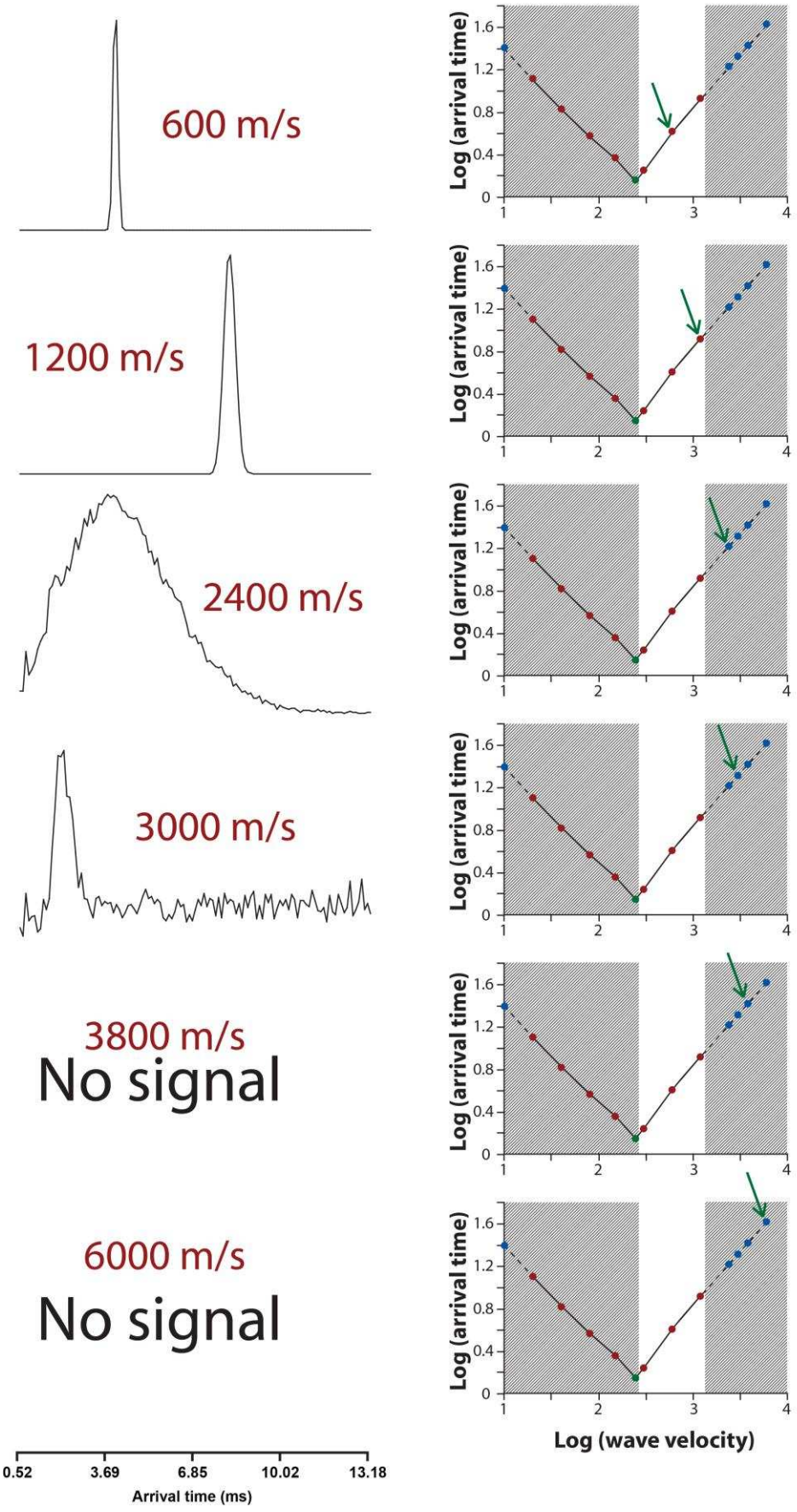
600 m/s
1200 m/s
2400 m/s
3000 m/s
3800 m/s
No signal
6000 m/s
No signal
0.52
3.69
6.85
10.02
13.18
Arrival time (ms)
Log (arrival time)
Log (wave velocity)

**S4.** Survival yields (SY), drift times (DT) and estimated effective temperature increases (based on Equations 1 and 3 in the main text) due to field heating induced by the traveling wave ($\Delta T_{IM}$) for the four CsI clusters studied, for some of the IM wave height/velocity combinations in Figures 1 and S2. The last columns in Tables (b), (c) and (d) show the drift time(s) observed for some of the smaller clusters released by field heating (N/A: no IM separation under these conditions and thus no discernible peak; no signal: ion absent or too low in abundance to determine DT). Measured drift time (marked with an asterisk) for (wave height = 22 V/wave velocity = 10 m/s) was not reliably measured due to roll-over; as a result, this value was entered manually (highlighted in bold), assuming (based on accurately measured $v_d$ at slightly higher wave velocities and wave height = 22 V) that $v_d = s$ under these conditions.

| $(CsI)_2Cs^+$ (652 Da) | | | | | | |
|---|---|---|---|---|---|---|
| **WH (V)** | **WV (m/s)** | **SY (%)** | **DT (ms)** | **$v_d$ (m/s)** | **$v^2$ ($m^2/s^2$)** | **$\Delta T_{IM}$ (K)** |
| 2 | 600 | 98.8 | N/A | N/A | N/A | N/A |
| 6 | 600 | 99.6 | N/A | N/A | N/A | N/A |
| 10 | 600 | 99.2 | 17.20 | 14.5 | 8721 | 228 |
| 14 | 600 | 98.9 | 9.15 | 27.3 | 16393 | 429 |
| 18 | 600 | 98.9 | 5.73 | 43.6 | 26178 | 684 |
| 22 | 10 | 33.2 | 3.20* | **10.0** | 100 | 3 |
| 22 | 20 | 35.8 | 12.79 | 19.5 | 1486 | 39 |
| 22 | 40 | 24.7 | 6.73 | 37.1 | 5333 | 139 |
| 22 | 80 | 63.0 | 3.75 | 66.7 | 16164 | 423 |
| 22 | 150 | 85.9 | 2.32 | 107.8 | 42614 | 1114 |
| 22 | 300 | 98.3 | 1.76 | 142.0 | 36765 | 961 |
| 22 | 600 | 98.4 | 4.08 | 61.3 | 35800 | 936 |
| 22 | 1200 | 98.4 | 8.38 | 29.8 | 8721 | 228 |
| 22 | 2400 | 97.8 | N/A | N/A | N/A | N/A |
| 22 | 3000 | 91.1 | N/A | N/A | N/A | N/A |
| 22 | 3800 | 0.0 | No signal | N/A | N/A | N/A |
| 22 | 6000 | 0.0 | No signal | N/A | N/A | N/A |
| 26 | 600 | 91.2 | 3.09 | 80.9 | 48544 | 1269 |
| 30 | 600 | 91.6 | 2.43 | 102.9 | 61728 | 1614 |
| 34 | 600 | 68.5 | 1.98 | 126.3 | 75758 | 1980 |
| 38 | 600 | 30.7 | 1.76 | 142.0 | 85227 | 2228 |

| $(CsI)_4Cs^+$ (1172 Da) | | | | | | | |
|---|---|---|---|---|---|---|---|
| **WH (V)** | **WV (m/s)** | **SY (%)** | **DT (ms)** | **$v_d$ (m/s)** | **$v^2$ ($m^2/s^2$)** | **$\Delta T_{IM}$ (K)** | **DT652 (ms)** |
| 2 | 600 | 91.9 | N/A | N/A | N/A | N/A | N/A |
| 6 | 600 | 92.9 | N/A | N/A | N/A | N/A | N/A |
| 10 | 600 | 94.1 | N/A | N/A | N/A | N/A | N/A |
| 14 | 600 | 86.1 | 9.04 | 27.7 | 16593 | 780 | 9.04 |
| 18 | 600 | 84.6 | 5.73 | 43.6 | 26178 | 1230 | 5.73 |
| 22 | 10 | 86.6 | 3.31* | **10.0** | 100 | 5 | 3.20 |
| 22 | 20 | 84.8 | 12.90 | 19.4 | 388 | 18 | 12.79 |
| 22 | 40 | 71.5 | 6.84 | 36.5 | 1462 | 69 | 6.84 |
| 22 | 80 | 80.6 | 3.75 | 66.7 | 5333 | 251 | 3.75 |
| 22 | 150 | 77.5 | 2.32 | 107.8 | 16164 | 759 | 2.32 |
| 22 | 300 | 83.0 | 3.31 | 75.5 | 22659 | 1065 | 1.76/3.31 |
| 22 | 600 | 82.5 | 6.84 | 36.5 | 21930 | 1030 | 4.08 |
| 22 | 1200 | 84.1 | 15.32 | 16.3 | 19582 | 920 | 8.38/15.44 |
| 22 | 2400 | 62.1 | N/A | N/A | N/A | N/A | N/A |
| 22 | 3000 | 0.0 | No signal | N/A | N/A | N/A | N/A |
| 22 | 3800 | 0.0 | No signal | N/A | N/A | N/A | No signal |
| 22 | 6000 | 0.0 | No signal | N/A | N/A | N/A | No signal |
| 26 | 600 | 82.8 | 5.07 | 49.3 | 29586 | 1390 | 3.09 |
| 30 | 600 | 84.2 | 3.97 | 63.0 | 37783 | 1775 | 2.43 |
| 34 | 600 | 84.1 | 3.20 | 78.1 | 46875 | 2202 | 1.98 |
| 38 | 600 | 84.8 | 2.65 | 94.3 | 56604 | 2660 | 1.76/2.65 |

| $(CsI)_6Cs^+$ (1692 Da) | | | | | | | | |
|---|---|---|---|---|---|---|---|---|
| **WH (V)** | **WV (m/s)** | **SY (%)** | **DT (ms)** | **$v_d$ (m/s)** | **$v^2$ ($m^2/s^2$)** | **$\Delta T_{IM}$ (K)** | **DT652 (ms)** | **DT1172 (m/s)** |
| 2 | 600 | 79.7 | N/A | N/A | N/A | N/A | N/A | N/A |
| 6 | 600 | 97.0 | N/A | N/A | N/A | N/A | N/A | N/A |
| 10 | 600 | 98.7 | N/A | N/A | N/A | N/A | 7.17/17.53 | N/A |
| 14 | 600 | 98.6 | 20.73 | 12.1 | 7236 | 491 | 9.26/15.66 | 14-21 |
| 18 | 600 | 98.6 | 12.90 | 19.4 | 11628 | 789 | 5.84 | 9.81/13.01 |
| 22 | 10 | 94.1 | 3.31* | **10.0** | 100 | 7 | 3.20 | 3.31 |
| 22 | 20 | 90.9 | 12.90 | 19.4 | 388 | 26 | 12.79 | 12.90 |
| 22 | 40 | 78.8 | 6.84 | 36.5 | 1462 | 99 | 6.84 | 6.84 |
| 22 | 80 | 98.5 | 3.75 | 66.7 | 5333 | 362 | N/A | 3.75 |
| 22 | 150 | 99.3 | 2.32 | 107.8 | 16164 | 1096 | 2.32 | 2.32 |
| 22 | 300 | 98.3 | 4.30 | 58.1 | 17442 | 1183 | 1.87 | 3.31/4.19 |
| 22 | 600 | 97.1 | 8.82 | 28.3 | 17007 | 1154 | 4.08/5.40 | 6.95/8.93 |
| 22 | 1200 | 92.5 | 21.72 | 11.5 | 13812 | 937 | 8.49 | 15.32/21.72 |
| 22 | 2400 | 39.9 | N/A | N/A | N/A | N/A | 3.31/4.74 | N/A |
| 22 | 3000 | 0.0 | No signal | N/A | N/A | N/A | 2.65/3.09 | No signal |
| 22 | 3800 | 0.0 | No signal | N/A | N/A | N/A | No signal | No signal |
| 22 | 6000 | 0.0 | No signal | N/A | N/A | N/A | No signal | No signal |
| 26 | 600 | 94.7 | 6.50 | 38.5 | 23077 | 1565 | 2.98 | 5.07/6.50 |
| 30 | 600 | 96.9 | 5.07 | 49.3 | 29586 | 2007 | 2.43 | 3.97/5.07 |
| 34 | 600 | 97.9 | 3.97 | 63.0 | 37783 | 2563 | 2.76 | 3.20/4.08 |
| 38 | 600 | 93.4 | 3.31 | 75.5 | 45317 | 3074 | 2.09 | 2.20/2.65/3.31 |

| $(CsI)_8Cs^+$ (2212 Da) | | | | | | | | | |
|---|---|---|---|---|---|---|---|---|---|
| **WH (V)** | **WV (m/s)** | **SY (%)** | **DT (ms)** | **$v_d$ (m/s)** | **$v^2$ ($m^2/s^2$)** | **$\Delta T_{IM}$ (K)** | **DT652 (ms)** | **DT1172 (ms)** | **DT1692 (ms)** |
| 2 | 600 | 0.0 | N/A | N/A | N/A | N/A | N/A | N/A | N/A |
| 6 | 600 | 93.8 | N/A | N/A | N/A | N/A | N/A | N/A | N/A |
| 10 | 600 | 94.5 | N/A | N/A | N/A | N/A | N/A | N/A | N/A |
| 14 | 600 | 95.4 | 18.08 | 13.8 | 8296 | 736 | 9.48 | 15.55 | 5.3/13.34/20.84 |
| 18 | 600 | 95.8 | 17.31 | 14.4 | 8666 | 768 | 5.62 | 9.70 | 8.49/12.90/17.31 |
| 22 | 10 | 62.9 | 3.31* | **10.0** | 100 | 9 | 2.02/3.20 | N/A | 3.31 |
| 22 | 20 | 69.0 | 12.90 | 19.4 | 388 | 34 | 12.90 | 12.90 | 12.90 |
| 22 | 40 | 50.3 | 6.84 | 36.5 | 1462 | 130 | 6.84 | 6.84 | 6.84 |
| 22 | 80 | 98.8 | 3.75 | 66.7 | 5333 | 473 | 3.64 | 3.75 | 3.75 |
| 22 | 150 | 99.4 | 2.32 | 107.8 | 16164 | 1433 | 2.32 | 2.32 | 2.32 |
| 22 | 300 | 96.7 | 5.62 | 44.5 | 13345 | 1183 | 1.76 | 3.53 | 2.54/4.19/5.62 |
| 22 | 600 | 94.1 | 11.91 | 21.0 | 12594 | 1117 | 4.08 | 6.95 | 5.73/8.82/12.13 |
| 22 | 1200 | 91.2 | N/A | N/A | N/A | N/A | 8.49 | 15.44 | 15.99/21.45 |
| 22 | 2400 | 0.0 | No signal | N/A | N/A | N/A | 7.39 | No signal | No signal |
| 22 | 3000 | 0.0 | No signal | N/A | N/A | N/A | 2.65/3.09 | No signal | No signal |
| 22 | 3800 | 0.0 | No signal | N/A | N/A | N/A | No signal | No signal | No signal |
| 22 | 6000 | 0.0 | No signal | N/A | N/A | N/A | No signal | No signal | No signal |
| 26 | 600 | 95.4 | 8.71 | 28.7 | 17222 | 1527 | 2.98 | 5.18/8.71 | 4.30/6.50/8.71 |
| 30 | 600 | 97.1 | 6.61 | 37.8 | 22693 | 2012 | 2.43 | 3.97 | 3.31/5.07/6.73 |
| 34 | 600 | 95.9 | 5.92 | 42.2 | 25338 | 2247 | No signal | No signal | 2.65/3.97/5.40 |
| 38 | 600 | 97.7 | 4.41 | 56.7 | 34014 | 3016 | 1.76/2.32 | 2.54 | 2.32/3.31/4.41 |

**Figure S5.** Contour map showing survival yields of $(CsI)_6Cs^+$ (1692 Da) and $(CsI)_8Cs^+$ (2212 Da) across a wide range of different Trap T-wave conditions.

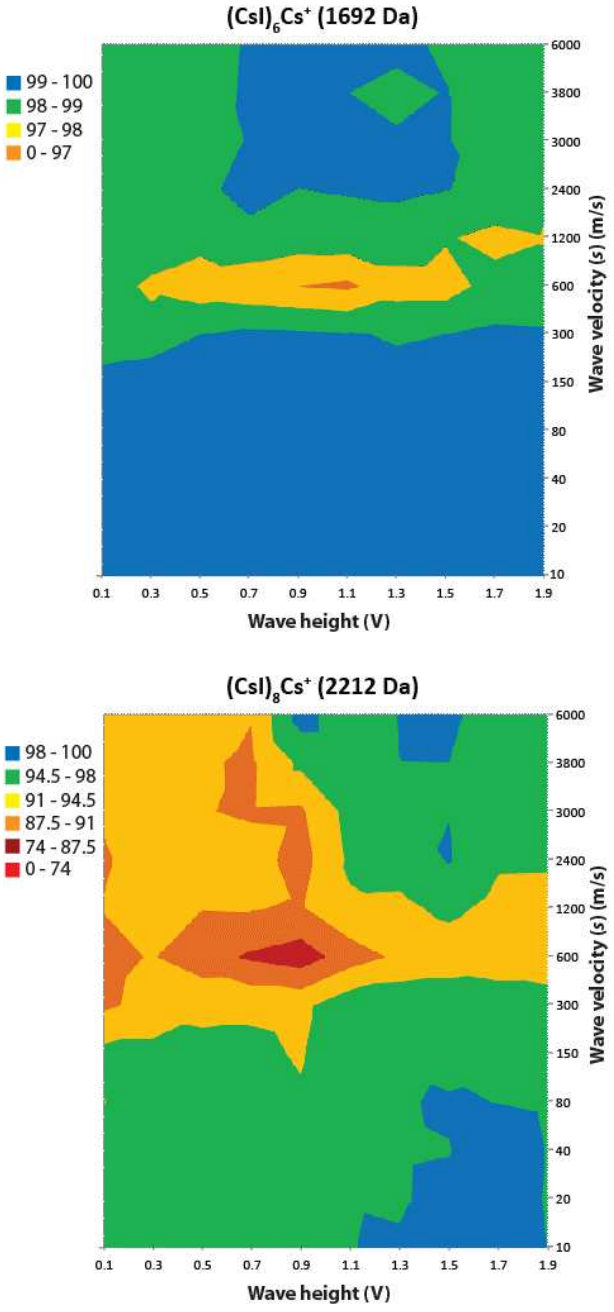

**S6.** Survival yields (SY) for the four CsI clusters studied, for some of the Trap wave height/velocity combinations in Figures 2 and S4.

| | | SY | | | |
|---|---|---|---|---|---|
| **WH (V)** | **WV (m/s)** | **$(CsI)_2Cs^+$ (652 Da)** | **$(CsI)_4Cs^+$ (1172 Da)** | **$(CsI)_6Cs^+$ (1692 Da)** | **$(CsI)_8Cs^+$ (2212 Da)** |
| 0.1 | 600 | 86.9 | 91.9 | 98.6 | 90.3 |
| 0.3 | 600 | 80.1 | 86.6 | 97.8 | 91.2 |
| 0.5 | 600 | 90.1 | 86.0 | 97.4 | 89.0 |
| 0.7 | 600 | 86.9 | 83.3 | 97.2 | 86.9 |
| 0.9 | 10 | 99.5 | 99.9 | 100.0 | 95.6 |
| 0.9 | 20 | 99.5 | 100.0 | 99.8 | 95.7 |
| 0.9 | 40 | 99.3 | 99.6 | 99.8 | 95.2 |
| 0.9 | 80 | 98.9 | 99.4 | 99.6 | 94.9 |
| 0.9 | 150 | 98.8 | 98.5 | 99.5 | 94.2 |
| 0.9 | 300 | 95.0 | 97.2 | 99.2 | 93.6 |
| 0.9 | 600 | 86.5 | 81.2 | 97.0 | 85.7 |
| 0.9 | 1200 | 57.3 | 84.9 | 98.5 | 90.7 |
| 0.9 | 2400 | 86.2 | 89.8 | 99.0 | 89.7 |
| 0.9 | 3000 | 85.7 | 90.7 | 99.2 | 90.5 |
| 0.9 | 3800 | 82.1 | 95.9 | 99.1 | 95.2 |
| 0.9 | 6000 | 85.4 | 94.8 | 99.3 | 99.5 |
| 1.1 | 600 | 85.6 | 88.6 | 96.8 | 89.3 |
| 1.3 | 600 | 84.8 | 84.8 | 97.6 | 91.7 |
| 1.5 | 600 | 83.4 | 88.3 | 97.6 | 92.4 |
| 1.7 | 600 | 83.0 | 90.3 | 98.4 | 91.2 |
| 1.9 | 600 | 83.5 | 91.1 | 98.3 | 91.3 |

**S7.** ETD spectra of 9+ ubiquitin, acquired using a Trap T-wave height of 0.3 V and velocities of 150, 300, and 1200 m/s (no supplemental activation applied). Note that non-dissociative charge reduction dominates in the top spectrum (indicating a very short reaction time), whereas the bottom spectrum shows only one (extensively) charge-reduced state and almost exclusively singly charged fragments (both indicating a very long reaction time) and possesses a fairly low signal-to-noise ratio. Intermediate wave velocities (middle spectrum) are optimal for efficient detection of fragments at a high S/N ratio.